Modeling Handball-Induced Head Injuries

Developing a Model of a Handball for Evaluating Concussion Risk and the Effectiveness of Protective Gear for Handball Players

Master's thesis in Applied Mechanics

Arvid Johansson
Cyrus Nilsson

DEPARTMENT OF MECHANICS AND MARITIME SCIENCES

CHALMERS UNIVERSITY OF TECHNOLOGY
Gothenburg, Sweden 2025
www.chalmers.se

Master's Thesis in Applied Mechanics

Modeling Handball-Induced Head Injuries

Developing a Model of a Handball for Evaluating Concussion Risk and the Effectiveness of Protective Gear for Handball Players

Arvid Johansson
Cyrus Nilsson

CHALMERS
UNIVERSITY OF TECHNOLOGY

Department of Mechanics and Maritime Sciences
Division of Mechanical Engineering
Chalmers University of Technology
Gothenburg, Sweden 2025

Modeling and Simulating Handball-Induced Head Injuries
Evaluating Concussion Risk for Handball Players
Arvid Johansson
Cyrus Nilsson

Supervisor: Johan Davidsson, Department of Mechanics and Maritime Sciences
Industrial supervisor: Niklas Jansson, FS Dynamics
Industrial supervisor: Erik Svenning, FS Dynamics
Examiner: Johan Iraeus, Department of Mechanics and Maritime Sciences

Master's Thesis 2025
Department of Mechanics and Maritime Sciences
Chalmers University of Technology
SE-412 96 Gothenburg
Sweden
Telephone +46 31 772 1000

Cover: FE simulation result of Human Body Model hit by a handball

Typeset in LaTeX
Gothenburg, Sweden 2025

Modeling and Simulating Handball-Induced Head Injuries
Evaluating Concussion Risk for Handball Players
Arvid Johansson
Cyrus Nilsson
Department of Mechanics and Maritime Sciences
Division of Mechanical Engineering
Chalmers University of Technology

Abstract

Concussions are a major problem in many sports, and handball is no exception. While some efforts have been made to reduce the prevalence of concussions, the risks remain high, with several cases of players ending their careers in their early twenties due to repeated concussions. Despite this, players are not allowed any form of head gear or other protection by the International Handball Federation rule set.

This thesis developed an explicit Finite Element handball model for LS Dyna based on coupon material test data and dynamic impact test data. The risk of concussion for a handball player was then estimated by modeling ball-to-head contacts using the new ball model and a state-of-the-art Human Body Model (HBM), the VIVA+, and the Injury Risk Function (IRF) DAMAGE. The use of HBM and IRF in quantifying concussion risks is a well-established methodology, particularly in the automotive industry.

The standing average male VIVA+ model was used, modified to contain only head and neck, constrained at the lower neck. Four impact scenarios at 110 km/h were simulated, where results were used to quantify mild Traumatic Brain Injury (mTBI) risk for each scenario. Two of these impact scenarios were tested under varying coefficients of friction between ball and head, with and without a foam sliding layer, representing an abstraction of head protective gear. The risk of mTBI was estimated to 10 - 35 % without headgear. With headgear, the results indicate that a substantial reduction of up to 25 % for head-on impacts and 50 % for lateral impacts in mTBI risk can be achieved with the appropriate headgear design.

Keywords: Brain concussion, mild Traumatic Brain Injury (mTBI), Biomechanics, Handball, Sports related injury, Human Body Bodel (HBM), Injury Risk Function (IRF), Finite Element Modeling, LS-DYNA.

Acknowledgements

This thesis would not have been possible without the help, input and support from several people and organizations. We give our utmost thanks to:

- Supervisor Johan Davidsson for his deep engagement, availability and generous help throughout the project.
- Examiner Johan Iraeus for his role in the examination process and for contributing to the academic integrity of this thesis.
- Industrial supervisors Niklas Jansson and Erik Svenning for their guidance in material models, ANSA pre-processor, LS Dyna and FE simulations in general.
- FS Dynamics for their hospitality and giving us a great working environment.
- Professor Anders Ekberg for putting us into contact with RIK, their trainers, inviting us to a match and his general engagement in the project.
- Professor Roland Kádár and Postdoc Marko Bek from the Rheology Lab at Chalmers for allowing us to use the lab for material testing and assisting us with these tests.
- Researcher Jobin John for preparing a modified VIVA+ model for us.
- Anders Bernhardsson from DYNAmore for his excellent introduction course to LS Dyna and LS PrePost.
- The RIK players for their fantastic shots at the load cell during the physical tests and trainers Jasmin Zuta, Fikret Handan and Mikael Franzén for allowing us to disturb their training for these tests.
- Dan Bråse at Autoliv AB for borrowing us the load cell.
- Tommy Gundersen at Volvo Personvagnar for borrowing us the DeweSoft measuring system and high speed cameras.
- AirSite AB for allowing us to use their workshop and some materials for building the test rig.
- Plåtpressning AB for providing sheet metal for the test rig on very short notice.
- Prioritet Serneke Arena for allowing us to mount the test rig in their sports hall.
- Karin Brolin at Lightness by Design for sharing knowledge regarding foam materials and implementation of them in LS Dyna.
- Jonas Östh at Volvo Cars for verifying our DAMAGE values and pointing out an error in the AIS classifications.

Arvid Johansson, Cyrus Nilsson, Gothenburg, June 2025

List of Acronyms

Below is the list of acronyms that have been used throughout this thesis listed in alphabetical order:

AAAM	Association for the Advancement of Automotive Medicine
AIS	Abbreviated Injury Scale
CAE	Computer-Aided Engineering
COR	Coefficient of Restitution
CV	Control Volume
DAI	Diffuse Axonal Injury
DAMAGE	Diffuse Axonal Multi-Axis General Evaluation
DMA	Dynamic Mechanical Analysis
FE	Finite Element
FEM	Finite Element Method
FPS	Frames Per Second
HBM	Human Body Model
HSM	Hertz-Signorini-Moreau
LSTC	Livermore Software Technology Corporation
MIPS	Multi-directional Impact Protection System
mTBI(s)	mild Traumatic Brain Injury (Injuries)
RIK	Redbergslid Idrottsklubb
PSA	Prioritet Serneke Arena
SRF	Solid Rectangular Fixture
TTS	Time-Temperature Superposition
VHHI	VIVA+ Head-Handball Impact
VHSL	VIVA+ Headgear Sliding-Layer
WLF	Williams-Landel-Ferry

Nomenclature

Indices

i, j, k, l	Indices for index notation
e	Index for elastic component
v	Index for viscous component
m	Index for Ogden hyperelastic parameters
M	Amount of Ogden hyperelastic parameters
n	Index for Prony fit parameters
N	Amount of Prony fit parameters
in	Incoming (before impact with wall)
out	Outgoing (after impact with wall)

Parameters

σ_{ij}	Cauchy stress tensor
τ_{ij}	Kirchhoff stress tensor
ε_{ij}	Strain tensor
λ_i	Principal stretch
$\tilde{\lambda}_i$	Volumetric independent principal stretch
W	Strain energy
K	Bulk modulus
J	Relative volume change
μ_m, α_m	Ogden hyperelastic parameters
G_n, β_n, τ_n	Prony fit parameters
t, τ	Time and time integration variable
g_{ijkl}, g	Relaxation function
G'	Shear storage modulus
G''	Shear loss modulus
$\tan\delta$	Loss factor
v	Velocity
a, b, c, d	Weibull parameters
x	Tissue-level metrics
y	Kinematic-based metrics
P	Probability

Contents

List of Figures

List of Tables

1
Introduction

Brain injuries in sports is an increasingly studied topic among researchers and clinical professionals. Discussions regarding these injuries have led to rule changes in several sports, and handball is no exception, where a rule change in 2022 established penalties for shots to the goalkeeper's head [1]. This study is aimed at both researchers and players interested in what could be done to prevent life-long injuries or premature retirements among handball players. The study is a Master's thesis of 30 credits and a collaboration between FS Dynamics AB and Chalmers University of Technology.

1.1 Background

Handball is a sport in which two teams, each of seven players, compete over control of the ball and attempt to score by throwing the ball into the opposing team's goal. Shots are usually taken by throwing the ball with ones hand, although using ones arms, head, chest or upper legs is also allowed. A sort of glue, made for handball and known as resin, can be applied to ones hands to give a better grip of the ball, allowing harder and faster shots. There is a goalkeeper who has the task of preventing the ball from entering the goal. In doing so, the goalkeeper may use their entire body to block any incoming shots. This presents a risk of the ball impacting the goalkeepers head, which could result in injury including concussion. Players who experience multiple concussions may be at risk of permanent brain injuries [2], leading to some players electing to retire early instead. When studying the risk of head injuries for handball players it was found that 39 % of 234 questioned players have had at least one handball related head injury, of which 62 % have had more than one [3].

In many other sports where head injuries are a risk, especially for goal keepers, the use of a helmet or other protective gear is common. In handball, no protective head gear is allowed under the current rule set [4]. Due to the high prevalence of concussion, there is a need for studying both the risk of concussion and methods for reducing it. One study by V. Sturesson, P. Marforio, A. Reuter, et al. [5] looked at prevention strategies such as: informing players about risk, reviewing rules and improving player strategies. An alternative is to model the impact between the head and the handball to quantify concussion risks for arbitrary impact scenarios. The use of Human Body Models (HBM) for injury risk quantification, including brain injuries, is however widespread, especially in the automotive industry [6]. HBMs are commonly used together with Injury Risk Functions (IRF) to predict concussion risk, clinically referred to as mild Traumatic Brain Injury (mTBI) risk.

1.2 Aim

Head injuries like concussions are a major problem in handball. To address this problem, the aim of this study was to enable quantification of injury risks when players are hit in the head by handballs. Moreover, the influence of protective gear on this risk was also studied, to determine if using protective gear would reduce the prevalence of concussions among handball players. The objectives of this thesis is thus to,

- Utilize the VIVA+ HBM and the DAMAGE IRF to quantify mTBI risk with different or no head protective gear.
- Create a handball FE model to use as an impactor when quantifying the mTBI risk.
- Collect dynamic impact test data to evaluate accuracy of the handball model compared to real handballs.
- Conduct coupon material testing to base the material models of the FE handball on.

1.3 Delimitations

The handball model will be accurate in the sense of simulating external interactions, like impacts to an HBM head. Internal factors, such as rupture or other damage to the ball, will not be addressed in this study. The handball resin will not be specifically modeled other than modeling the friction of the handball.

Only the head and neck components of the VIVA+ HBM will be included, to reduce computational cost. Only the male version of the VIVA+ HBM will be used. Handball sizes differ between male/female players, with the larger handballs being used by males. The handball model created in this study could be scaled for future studies that include a female HBM.

Two different shot scenarios will be the focus of the impact modeling. The FE model will be simulated for a single ball pressure, and the effects of varying pressure will not be studied.

The only injury criterion considered in this study is Diffuse Axonal Multi-Axis General Evaluation (DAMAGE).

2
Theory

There are two distinct areas in this study, modeling the handball and its interactions, and modeling the human head and its response. They share a common modeling approach of using the Finite Element Method (FEM), but they consist of very different materials and require different theory to describe.

2.1 Finite element modeling

Finite element method is a numerical method for solving differential equations that describe physical phenomena, such as heat transfer and structural deformations. The method works by discretizing the problem domain into small subdomains, known as finite elements. Each element consists of several nodes, in which relevant equations are solved individually for nodal quantities, like nodal displacement or nodal velocities. Nodal results are then approximated over the elements and the results are combined to form a global solution. This approach makes it possible to tackle complex problems with irregular geometries, non-linear behaviors, and varying boundary conditions [7].

Two major solution techniques in FEM are implicit and explicit solvers. Implicit solvers are common for static problems or problems with low amounts of dynamics. Implicit solvers find solutions by using the current state and future state. Since the future state is generally unknown, this means a system of equations for the future state must be solved before a solution can be acquired. Explicit solvers are common for dynamic problems, or problems with fast and large deformations. Explicit solvers base their solutions only on the current state, and as such do not need to solve a large equation system for every state. This makes them faster per solution but they might require shorter time steps to achieve stable solutions [8].

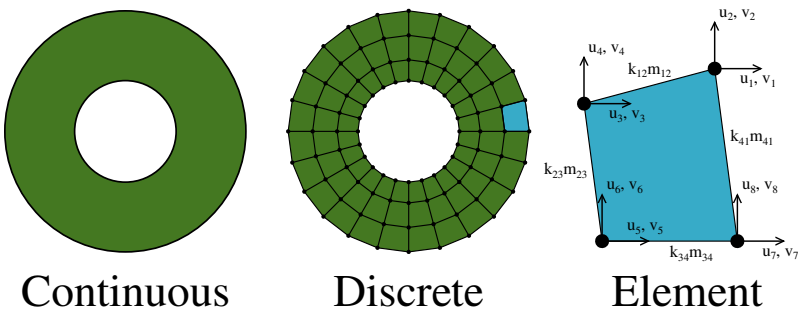

Figure 2.1: Discretization of a continuous domain into quadrilateral elements

2.2 LS Dyna

LS Dyna is a commonly used simulation software for Computer-Aided Engineering (CAE), developed by Livermore Software Technology Corporation (LSTC) owned by Ansys, Inc., offering both implicit and explicit solvers. A wide range of materials, contact options and element formulations are available. These features are included in the LS Dyna FE structure in a form known as keywords or cards. When these keywords are mentioned in text they will be presented as `KEYWORD_NAME`. For further reading about any specific keyword, refer to the LS Dyna keyword manuals, volume I and II [9].

2.2.1 Element formulations

There is a vast amount of element formulations available in FEM, but they can generally be said to differ in a few key aspects: Dimensionality, Order, Integration and Geometry.

In regards to dimensionality, the key is how many dimensions that can be abstracted without significant loss of accuracy, for example: beam elements (1D), shell elements (2D) and solid elements (3D). The element's order represents the number of nodes in the element and the order of the interpolating functions (shape functions) between nodes. Solid elements are commonly referred to by the number of faces they have, a *hexahedral* solid element has six faces. Common solid element geometries are tetrahedrons, pentahedrons and hexahedrons [10, ch.4].

Finally, the integration scheme determines for how many points (and where) integration is done. The integration method used is usually Gauss Quadrature, which is what is used in LS Dyna, but with varying number of points [11]. The varying number of integration points leads to the possibility of under-integrating elements versus fully integrating them. Full integration can lead to better accuracy, however it can cause locking problems for lower order elements. Full integration is also very costly, and in the same way that dimensionality can be sacrificed for lighter computations, so too can integration. LS Dyna contains elements with one-point integration, selective reduced integration or full integration. Selective reduced integration attempts to strike a balance between the one-point and full options [10, ch.4].

2.2.2 Contact mechanics

Contact problems arise when objects, or in the case of FEM; elements and nodes, interact by coming into contact with each other. Contact problems vary in their complexity, but are almost always non-linear due to the area in contact generally being unknown. Several solution algorithms exist that treat contact mechanics, but due to the complex nature of contacts there is no universal solution that fits all cases [12, ch.1].

2.2.2.1 Penalty-based contact formulations

The penalty method is a widely used contact algorithm in FEM, and is described here as by P. Wriggers [12, ch.2]. The method is based on placing springs between all nodes in contact. These springs exert a force to resist further penetration, thus *penalizing* the movement of nodes on the contact surface. A conceptual view is shown in Figure 2.2 where a node approaches some surface, after which the node's movement becomes penalized by a resisting spring.

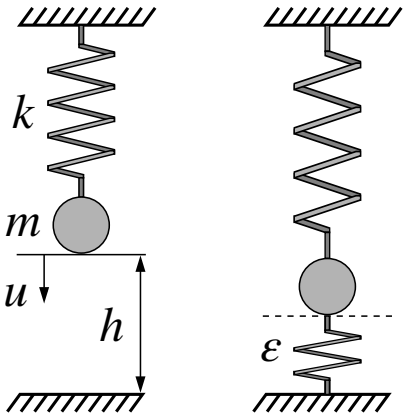

Figure 2.2: Abstracted spring and node representation of a penalty based contact

For the case in the figure above, a reaction force R_N can be formulated as,

$$R_N = \varepsilon c(u) \tag{2.1}$$

where ε is the penalty stiffness, c is the constraint and u the nodal displacement. The constraint c determines if the force is active or not, which is important to fulfill the Hertz-Signorini-Moreau (HSM) condition. This condition ensures that the contact does not transmit tensile forces, bodies do not penetrate, and that the contact force is only active for bodies in active contact. The HSM condition states that,

$$c(u) \geq 0\,, \quad R_N \leq 0 \text{ and } R_N c(u) = 0 \tag{2.2}$$

A penalty type constraint for the case in Figure 2.2 that satisfies HSM can be formulated as,

$$c(u) = h - u = \frac{kh - mg}{k + \varepsilon} \tag{2.3}$$

where k is the nodal stiffness, m the nodal mass, h the height from the surface.

LS Dyna contains four implementations of the penalty algorithm, the choice of which is made by the `SOFT` parameter or the choice of `MORTAR` contacts. These are all far more complex than what has been presented in this section, but they all build on applying springs in contacts to penalize penetrations. For further definitions, refer to the LS Dyna theory manual on contacts [10, ch.29].

2.2.2.2 Coulomb friction

Friction is a part of contact mechanics, but the purpose is different than that which has been discussed earlier, where the purpose was to prevent penetrations into materials (normal contact). Tangential contact forces also exist, referred to as frictional forces. The most common theory for describing friction is Coulomb friction,

$$F_y = \mu F_n \tag{2.4}$$

where F_y is the yielding frictional force, μ is the coefficient of friction and F_n the normal force. The force F_y is the maximum possible frictional force. If the required force for equilibrium exceeds this value, sliding will occur with the frictional force constant at F_y. If instead the force is lower, the actual frictional force will be lower as well [12, ch.5][10, ch.29].

2.2.3 Gas pressure control volumes

LS Dyna contains a wide range of methods for gas-inflated volumes, commonly used for modeling tires and airbags. However, there are general models that can be used to model arbitrary gas-filled volumes (like a handball), known as Control Volumes (CV), in which a gas exerts a pressure onto the surface of the CV. One commonly used equation for computing the pressure is the Gamma Law Gas Equation of State [10],

$$p = (\gamma - 1)\,\rho e \tag{2.5}$$

where p is the pressure inside the CV, γ is the ratio of specific heats, ρ is the gas density and e is the specific internal energy of the gas. Any change to pressure is considered isentropic, i.e. completely reversible and without heat transfer (adiabatic). As such the density for any state can be computed by isentropic ideal gas relations [13].

The initial specific internal energy e_0 is calculated first as 2.6, while any following variations are calculated by a change in volume v leading to a change internal energy e according to 2.7. Note that p_0 is the initial gauge pressure inside the CV, while p_e is the external pressure outside the CV (for example atmospheric pressure).

$$e_0 = \frac{p_0 + p_e}{\rho_0\,(\gamma - 1)} \tag{2.6}$$

$$e_2 = e_1 \left(\frac{v_2}{v_1}\right)^{(1-k)} \tag{2.7}$$

2.2.4 Dynamic relaxation

Introducing pressurized cavities or any other initial forces can put a model in a state where it is not initially in equilibrium. For example, pressurizing a sphere will cause it to expand, this requires equations to be solved for the expansion. If this is not done, the initial model state is not in equilibrium. This can cause oscillations

unless managed. One method of managing this is dynamic relaxation, where a static pre-computation is done to deform the model towards equilibrium. After this, any initial velocities are applied and the actual problem is solved with dynamic effects [14].

2.3 Material mechanics

Handballs are made out of leather or synthetic materials [15], where synthetic materials are most prevalent. These synthetic materials are polymers whose microstructure gives them non-linear behavior, which require several different material theories to model. This section introduces polymers, describes elastic and viscoelastic material behavior, and defines methods for testing and measuring these behaviors in experiments. Note that some definitions made in this section assumes a static problem for simplicity, in a dynamic simulation more variables are time dependent.

2.3.1 Polymeric materials

Polymers consist of long molecular chains of repeating structures. These chains create a vast network of linked or entangled chains. Molecules within one chain are strongly connected with covalent bonds. Chain to chain interaction is generally much weaker, and depends on the van der Waals force. The entangled structure creates a highly varying microstructure during loading, leading to non-linear behavior as the network of chains untangle. Movements of the chains is not instantaneous, and the timescales involved can vary from milliseconds to years depending on the type of polymer, temperature, amount of deformation and rate of deformation [16, ch.1].

The loaded state of a material can be explained with two parameters. The material deformation (strain, ε, unit: unitless/percent), and the material loading (stress, σ, unit: pressure). In this report, and for the polymeric material models used in LS Dyna, the stress tensor σ_{ij} is split into two separate parts: an elastic part σ^e_{ij} and a viscous (or viscoelastic) part σ^v_{ij} [9]. These parts will be explained more in depth in the next two sections.

An example of an arbitrary polymeric material is shown in Figure 2.3. Timescales and the amount of relaxation can vary wildly between different polymers. Only the viscous part is time dependent and will disappear given enough time. The elastic part is constant and remains indefinitely, given that the strain remains constant (if it changes, the problem is dynamic, and both stress components are time dependent). The result of this is that the material's internal loading relaxes with time [16, ch.6].

$$\sigma_{ij}(t) = \sigma^e_{ij} + \sigma^v_{ij}(t) \tag{2.8}$$

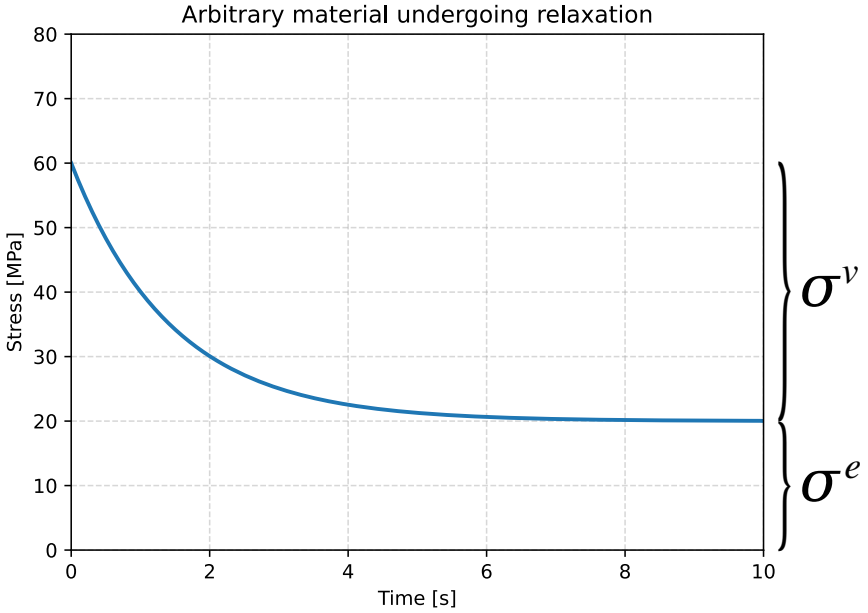

Figure 2.3: An arbitrary polymeric material relaxing after a constant strain ε was applied. The strain does not change with time in this case

2.3.2 Elasticity

Elasticity relates the elastic deformation to the loading of a material. Elastic deformations imply that if the material is unloaded, it will return to its original shape. The simplest theory is linear elasticity, which relates stress and strain with a linear function. In this case the stress is just the strain multiplied by an elastic constant [17]. However, linear elasticity is not suited for polymeric materials. These require the concept of hyperelasticity.

Hyperelastic models use a strain-energy function W to define the stress-strain relationship. This function defines the area under the stress-strain curve for some strain level or other deformation measure, commonly principal stretches or strain invariants. There is a wide range of hyperelastic models available, and the formulation of the strain-energy function is generally what sets them apart [16, ch.5][18].

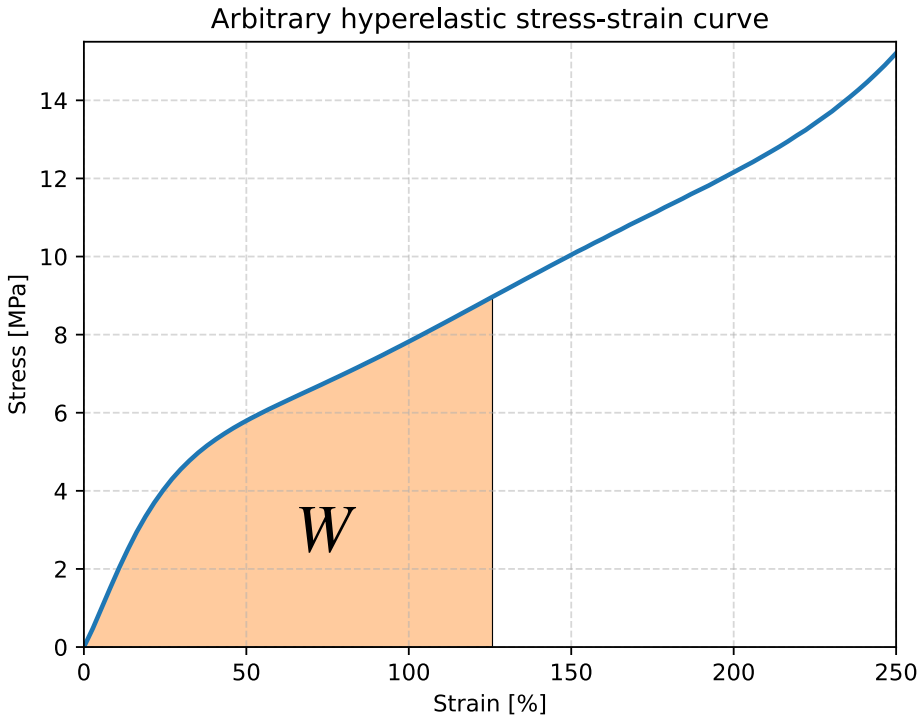

Figure 2.4: An arbitrary hyperelastic stress-strain curve. The strain energy W for 125 % strain is shown

The Ogden hyperelastic model developed by R.W. Ogden [19] is a hyperelastic model suited for rubber-like materials. It defines the strain-energy as a function of the principal stretches λ_i. The strain-energy function for an M-term Ogden model is defined in (2.9). The parameters μ_k and α_k must be fitted to test data or some other reference. Tests can be uniaxial, biaxial or in shear, and for some materials all of these may be required to properly describe the material behavior. However, for many materials a uniaxial test is sufficient [16, ch.5].

$$W\left(\tilde{\lambda}_1, \tilde{\lambda}_2, \tilde{\lambda}_3\right) = \sum_{m=1}^{M} \frac{\mu_m}{\alpha_m}\left(\tilde{\lambda}_1^{\alpha_m} + \tilde{\lambda}_2^{\alpha_m} + \tilde{\lambda}_3^{\alpha_m} - 3\right) + K\left(J-1\right) \tag{2.9}$$

This implementation of the strain energy function (2.9), and all other definitions leading to the Cauchy stress (2.13), are used in LS Dyna [10]. Note that the principal stretches marked with a tilde are independent from volumetric effects, see definition (2.10). Also, let a_m be the sum of the volumetric independent principal stretches exponentiated by the α parameter. Lastly let J be the relative volume change and K the bulk modulus.

$$\tilde{\lambda}_i = \frac{\lambda_i}{J^{1/3}} \quad , \quad a_m = \tilde{\lambda}_1^{\alpha_m} + \tilde{\lambda}_2^{\alpha_m} + \tilde{\lambda}_3^{\alpha_m} \quad , \quad J = \lambda_1\lambda_2\lambda_3 \tag{2.10}$$

The principal Kirchhoff stress τ_{ii}^E is then given as

$$\tau_{ii}^E = \lambda_i \frac{\partial W}{\partial \lambda_i} = \sum_{m=1}^{M} \mu_m \left(\tilde{\lambda}_i^{\alpha_m} - \frac{1}{3}a_m\right) + K\left(J-1\right) \tag{2.11}$$

The principal Kirchhoff stress is transformed by LS Dyna into standard basis by the components of the orthogonal tensor of eigenvectors

$$\tau_{ij} = q_{ik}q_{jl}\tau_{kl}^E \tag{2.12}$$

The Kirchhoff stress then gives the Cauchy stress as

$$\sigma_{ij}^e = J^{-1}\tau_{ij} \tag{2.13}$$

In LS Dyna, this stress is the elastic part σ_{ij}^e of the total stress.

2.3.3 Viscoelasticity

Viscous effects in materials add a stark contrast to the pure elastic behavior described so far. In elasticity, the way that a material was loaded is not important, only the current state is of importance for the material response. With the addition of viscosity, the material gains a sort of memory; earlier states now influence the current and future states of the material [20, ch.1]. From the separation of the material stress state into elastic and viscous components, this section will treat the theory behind the viscous stress component.

To describe viscous effects in materials also showing elastic properties, the theory of viscoelasticity exists. Linear viscoelasticity is the simplest way to model this combined behavior, and has both been extensively studied and used [16, ch.6]. The linear viscoelastic formulation used in LS Dyna, for the Ogden material model, is shown below [9].

$$\sigma_{ij}^{v}(t) = \int_0^t g_{ijkl}(t-\tau)\frac{\partial \varepsilon_{kl}}{\partial \tau}\,\mathrm{d}\tau \tag{2.14}$$

The definition of the shear relaxation modulus $g(t)$ is the primary challenge in applying linear viscoelasticity. A common approach is to employ the Maxwell model which consists of a spring with stiffness G and dashpot with relaxation time τ. If N sets of Maxwell models are defined and combined with an elastic model, this is known as the Generalized Maxwell model, where each term represents one set of spring and dashpot. Key to this model is that, with time, the viscoelastic part of the stress relaxes to zero [21]. The right-most formulation is the formulation used in the LS Dyna Ogden material model [9].

$$g(t) = \sum_{n=1}^{N} G_n e^{-t/\tau_n} = \sum_{n=1}^{N} G_n e^{-\beta_n t} \tag{2.15}$$

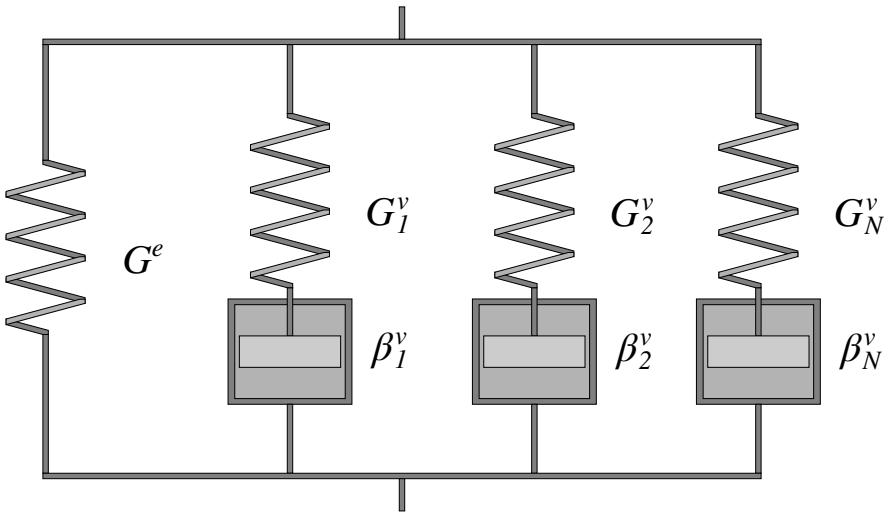

Figure 2.5: The Generalized Maxwell model, note the elastic stiffness G^e and the sets of Maxwell viscoelastic spring-dampers G_n^v, β_n^v

2.3.4 Tensile testing

Tensile testing is one of the most commonly employed types of material tests. A material sample is mounted between two clamps, and one of the two clamps are actuated to move, pulling on the sample. The movement introduces a strain into the sample, which results in a stress. By measuring the displacement of the clamp, and converting the signal from a strain gauge mounted in series with one of the clamps, a relationship between force and displacement can be produced. With known dimensions of the material specimen, this can be converted into a stress-strain relationship, which is the basis of most material models [22].

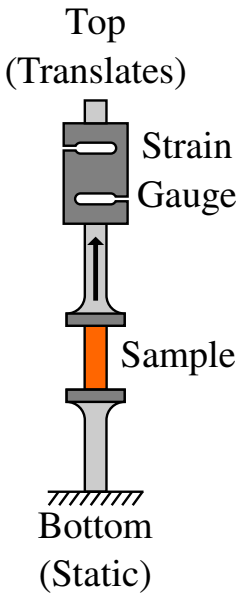

Figure 2.6: Tensile setup

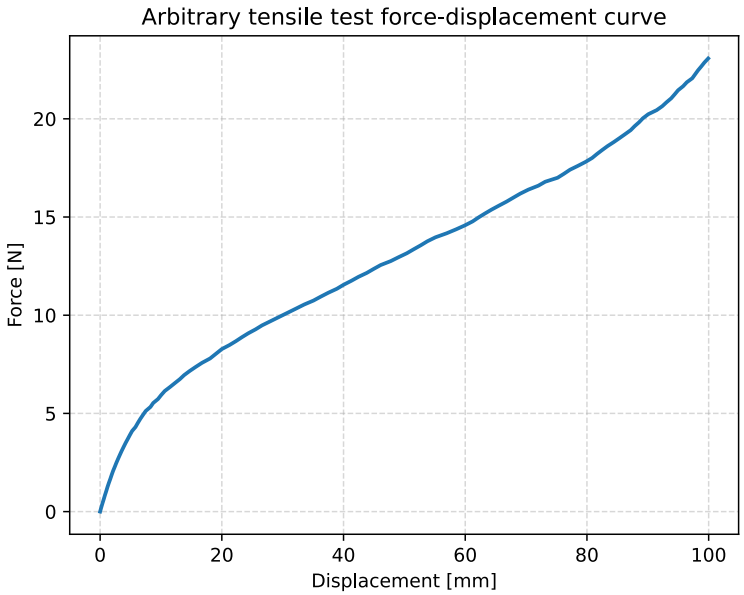

Figure 2.7: An arbitrary force-displacement curve for some material, produced by a tensile test

2.3.5 Dynamic Mechanical Analysis

An extensively used testing methodology for polymers is Dynamic Mechanical Analysis (DMA). The dynamic properties are studied by applying a cyclic uniaxial strain into a material sample for the mode of interest: tension, bending or shear. The results are often presented as the response to a strain amplitude ε (for an amplitude sweep) or a frequency ω (for a frequency sweep), where the response is the dynamic moduli, which in the case of shear are: Storage Modulus G' and Loss Modulus G''. Storage modulus represents the stored energy during the load phase, while loss modulus represents the dissipated energy during the load phase. Thus, storage modulus can be seen as the elastic response (spring in Maxwell model) and the loss modulus as the damping response (damper in Maxwell model), both forming the viscoelastic response [21].

When performing DMA on a viscoelastic material, a phase lag δ between the applied strain and measured stress can be observed, see Figure 2.9. The loss factor, defined in equation 2.16, is a measure of the material's damping behavior. For an ideally

elastic material ($\delta = 0$), and no elastic energy is lost. For an ideally viscous material ($\delta = 90°$), leading to a complete inability to store elastic energy [21][23].

$$\tan \delta = \frac{G''(\omega)}{G'(\omega)} \tag{2.16}$$

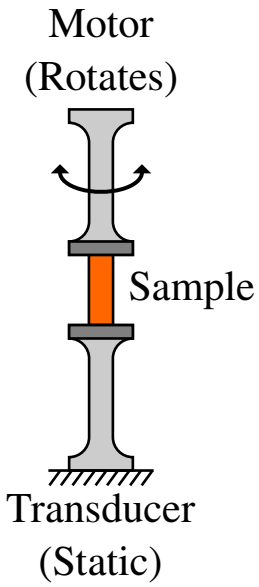

Figure 2.8: DMA setup

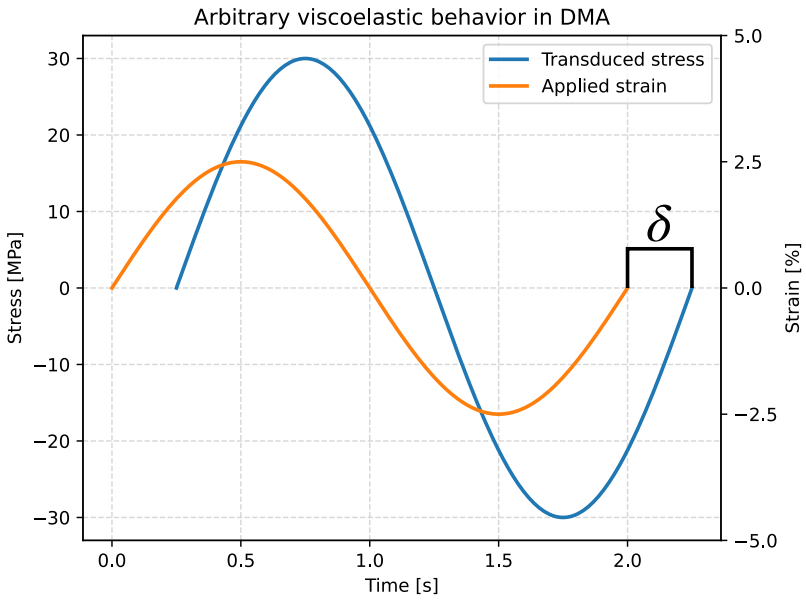

Figure 2.9: Phase lag for a viscoelastic material

2.3.5.1 Time-Temperature Superposition

When viscoelastic effects are measured at different temperatures for some range of frequencies, the temperature dependent data can be shifted in frequency, or superimposed, into a so called master curve. This is highly useful, as testing machines usually have strict limitations on their frequency range, while temperature is an easily controlled variable with a more generous allowable range. The method is known as the Time-Temperature Superposition (TTS) principle, which allows establishing a material master curve for some reference temperature T_{ref}. A master curve describes the viscoelastic behavior over a range of frequencies when a material is at the temperature T_{ref}. To establish a master curve for a viscoelastic material, multiple DMA tests are run in a specified frequency range for several temperatures. By using shift factors, TTS allows shifting the data at the experimental temperature onto the reference temperature, extending the total frequency range. Ideally, only horizontal shifting is required, but material nonlinearities, residual stresses or other error sources can cause slight vertical shifting to be needed as well. The Williams-Landel-Ferry equation (WLF) is widely used to determine horizontal a_T and vertical b_T shift factors, which are defined in equation 2.17 and 2.18 respectively [24, ch.5].

$$\log a_T = \frac{-C_1 (T - T_{ref})}{C_2 + T - T_{ref}} \tag{2.17}$$

$$b_T(T;T_{ref}) = \frac{T_{ref}\rho(T_{ref})}{T\rho(T)} \tag{2.18}$$

Where C_1 and C_2 are material parameters, these are adjusted until the shifted curves achieve best possible fit, ρ is the density of the viscoelastic material, T_{ref} is the reference temperature and T is the test temperature of the data to be shifted.

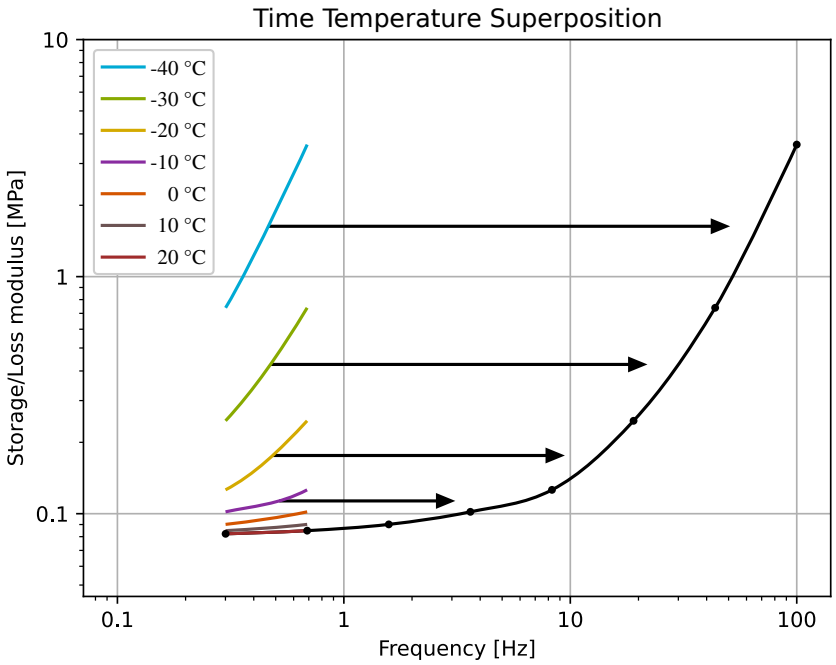

Figure 2.10: Example showing TTS, test data comes from lower frequencies with highly varying temperature and is then shifted horizontally to fit

2.3.5.2 Time discretization of dynamic moduli (Prony series)

The dynamic moduli $G'(\omega)$ and $G''(\omega)$ are relatively easy to measure with the correct equipment but difficult to interpret and apply to a material model, as they are functions of frequency. The time-discrete linear relaxation modulus $g(t)$ can directly be used in a viscoelastic model according to (2.14) and is supported in most simulation software, but is generally not a property measured by testing equipment. A way of converting between dynamic moduli and relaxation modulus is thus needed. A technique presented by M. Baumgaertel and H.H. Winter is presented here [25].

The technique involves curve fitting the measured dynamic moduli to long-term shear modulus G_0, and N constants G_i and τ_i to equation (2.19) or (2.20). These constants are then reused in the equation for the Generalized Maxwell model (2.15), also consisting of N terms. The resulting series of Maxwell elements is also referred to as a Prony series [26]. The regression is most commonly applied on the storage modulus and not the loss modulus, as the storage modulus determines the dominant

behavior and yields the best fit [21].

Note that the constant term G_0 is only used for the curve fit. The effects of G_0 are covered by the elastic parts of the stress, the viscous stress must relax to zero with time. The G_0 term is thus simply left out of the resulting Prony series used in the LS Dyna material model.

$$G'(\omega) = G_0 + \sum_{i=1}^{N} G_i \frac{(\omega\tau_i)^2}{1 + (\omega\tau_i)^2} \tag{2.19}$$

$$G''(\omega) = \sum_{i=1}^{N} G_i \frac{\omega\tau_i}{1 + (\omega\tau_i)^2} \tag{2.20}$$

2.4 Human body modeling and injury assessment

Human Body Modeling refers to the development and application of detailed computational representations of the human anatomy. These models are widely utilized in the automotive industry for crash safety research [27], but has also been used for studying injuries in sports [28]. There are several models available and they generally have some focus towards a specific sort of injury.

2.4.1 VIVA+ Human body model

VIVA+ is one available open-source HBM, developed with respect to finding an optimal level of anatomical accuracy that provides manageable computational cost [29]. Several publications on validation and application of the model exist [30]. These applications of VIVA+ generally involve extracting results to be used for predicting injuries using different injury criteria.

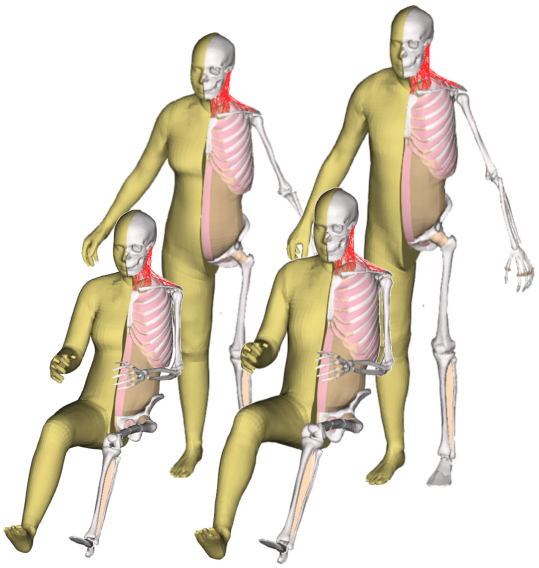

Figure 2.11: The VIVA+ HBM model, female and male versions

Image source: [31] under CC BY 4.0

2.4.2 Diffuse Axonal Multi-Axis General Evaluation

One such criteria to determine head injuries is the Diffuse Axonal Multi-Axis General Evaluation (DAMAGE) criteria, which is a rotational injury criterion developed to assess the risk of Diffuse Axonal Injury (DAI), such as concussions and other mild Traumatic Brain Injuries (mTBIs).

The DAMAGE value is derived from time-dependent angular accelerations and correlates closely with brain tissue strains as predicted by validated finite element models. This multi-axial approach captures the complex shear loading conditions responsible for axonal deformation, causing mTBIs. Wu et al. [32] found DAMAGE

to outperform traditional rotational metrics in predicting strain-based brain injury outcomes across human and non-human primate datasets.

2.4.3 Abbreviated Injury Scale

The Abbreviated Injury Scale (AIS) is a standardized, anatomy-based system for assessing and ranking the severity of individual injuries. Developed by the Association for the Advancement of Automotive Medicine (AAAM), the AIS provides a consensus derived, scale from one to six, where one denotes a minor injury and six indicates a maximal, currently untreatable injury [33]. In automotive crash safety and sports biomechanics, mTBIs—notably concussions—are of significant interest. On the AIS, mTBIs are typically classified as AIS 2, representing minor to moderate head injuries [34].

2.4.3.1 Weibull Distribution in Injury Risk Modeling

Injury risk functions are commonly used to estimate the probability of sustaining an injury based on biomechanical input variables, such as rotational acceleration. For predicting the risk of concussions, the Weibull distribution is frequently employed [32]. The cumulative Weibull risk function is defined as,

$$P_{injury} = 1 - e^{\left(-e^{\left(\frac{1}{b}+\ln x-\frac{a}{b}\right)}\right)} \tag{2.21}$$

where a and b are coefficients corresponding to the shape and scale parameters in the Weibull distribution, and x is the tissue-level injury metric. The kinematic-based metrics *(y)*, such as DAMAGE value, can by linear regression be determined from tissue-level metrics *(x)* using equation 2.22,

$$y = cx + d \tag{2.22}$$

Using the parameters a = *-0.9314*, b = *0.2452*, c = *0.957* and d = *0.017* for AIS 2, found in [32], a complete injury risk evaluation can be done. This allows the use of simulation derived DAMAGE values to estimate the risk of AIS 2 through statistical models.

2.4.4 Concussions

Concussions are a common form of mTBI, frequently occurring in sports. They result from biomechanical forces transmitted to the head, leading to functional disturbances in brain activity. Clinically, concussions are diagnosed based on a constellation of symptoms, including nausea, memory loss, headache and loss of consciousness [35].

2.4.4.1 Mechanisms of Injury

Concussions are typically induced by direct impacts to the head or by indirect forces applied to the body that propagate to the head. Notably, concussions have been

shown in correlation with changes in angular velocity of the brain [35].

Head kinematics during impacts can be classified into linear and rotational motions. While linear accelerations tend to produce injuries to a localized region of the brain, rotational accelerations are associated with more widespread brain injuries. Widespread injuries poses a higher concussion risk than localized injuries [36]. Additionally, the human head exhibits varying sensitivity to rotational accelerations about the different anatomical axes [37].

2.4.4.2 Recovery and Long-Term Risks

The incidence of a concussion increases the risk of additional concussive injuries, and repeated occurrences may result in cumulative damage or possibly permanent brain injuries. A single concussion may necessitate a rehabilitation period of up to four weeks before an individual is cleared to resume full training [3].

2.4.5 Protection gear mechanisms

Protective gear, such as helmets, are engineered to mitigate head injuries by reducing linear and rotational forces transmitted to the head. Two primary protective strategies employed are energy absorption through damping materials and reduction of rotational acceleration via sliding interfaces.

2.4.5.1 Damping materials

Helmets often incorporate damping layers made out of materials such as foams. These materials absorb energy from the impact by deforming when loaded, thereby reducing transmitted forces to the head. Advanced materials have been shown to significantly reduce linear accelerations across various sports [38].

2.4.5.2 Sliding interfaces

To minimize rotational force, modern helmet designs increasingly integrate slip-plane technologies [39]. A widely used example is the Multi-directional Impact Protection System (MIPS), which introduces a low-friction layer that allows relative motion between the helmet shell and the head during oblique impacts [40]. This mechanism reduces rotational acceleration and associated brain strain by decoupling rotational energy from the skull. In a study performed by Yung et al. [41] the coefficient of friction for the sliding layers was set to 0.17.

3
Methodology

The study has some milestones for which the methodology has been separated. The study begins with material testing to determine inputs for the material models used in FE simulations. The study then focuses on experiments where data was collected from real handball shots. The next phase involves creating a complete model of the handball, with data from the previous sections being used both as input for the model and as reference for model validation. The last section treats the handball and HBM impacts, where injury risk functions are used to quantify the concussion risk for different impact scenarios.

3.1 Material testing

To develop an accurate FE model of the handball, material testing of the SELECT Solera V24 size 3 handball was conducted. By tensile testing and DMA the handball's elastic and viscoelastic behavior could be determined. The material tests was carried out in the Rheology laboratory at Chalmers with supervision from Postdoc Marko Bek from the Industrial and Materials Science Department.

The ball consists of four materials (cf. Figure 3.1) possessing very different characteristics. The outer layer is a polyurethane based synthetic leather. One layer inwards there is a relatively thick and dense foam layer. Another layer in is a woven synthetic fabric layer. These three layers are all adhered to each other and stick together. The innermost layer is a rubber air bladder that lies loose inside the ball and is not adhered to the other layers, but once inflated presses against the other layers. All these layers were tested individually.

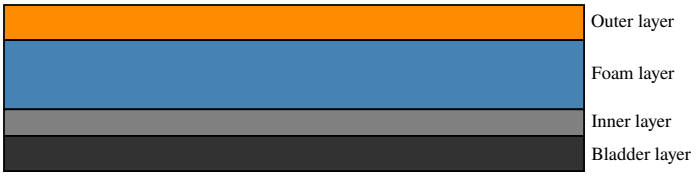

Figure 3.1: Composition of the SELECT Solera V24 Handball

3.1.1 Tensile test

To determine the elastic material behavior, tensile tests were conducted on each layer of the handball. These tests were carried out using a Zwick Z2.5 tensile tester, which has a maximum capacity of 2.5 kN, at a test speed of 50 $\frac{\text{mm}}{\text{min}}$, with a pre-load of 0.2 N. Each test was performed three to four times per layer to ensure consistency and reliability of the results.

During the tensile testing, test specimens were extracted from the Select Solera V24 handball, with dimensions as specified in the Appendix A. Specimens were of the same type as those used in the DMA, see Figure 3.3. Each specimen was then centered and vertically positioned in the hydraulic clamps of the tensile tester. Once the appropriate test speed and pre-load were set, the test was initiated and terminated upon rupture of the specimen. The data collected from the test was force and displacement.

The Inner layer was treated slightly differently from the other materials due to it having fiber directions, cf. Figure 3.2. One set of tensile tests were conducted along the fiber direction, and another set 45° offset from the fiber directions. The force-displacement relationship used for the material model was an average of these tests.

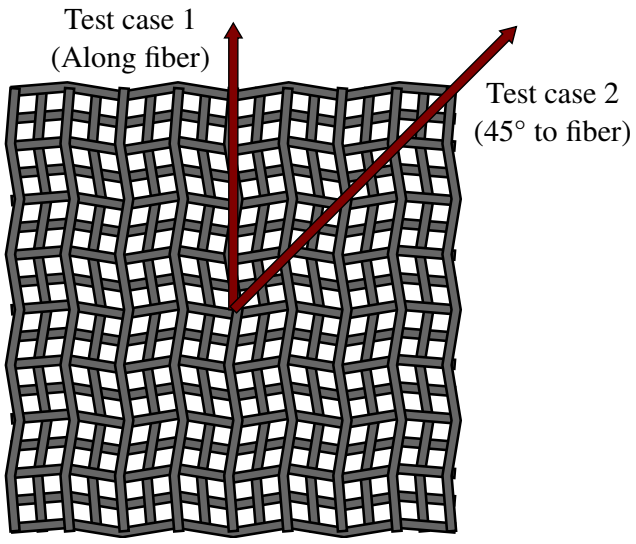

Figure 3.2: Visualization of the Inner layer, showing fiber and testing directions

3.1.1.1 Postprocessing and determination of elastic parameters

LS Dyna has the capability to automatically fit material models to force-displacement curves, there are however some requirements on the data for this to work. The force curve has to be monotonically increasing with increasing displacement, and while this is generally the case, during high force applications the sample might slip slightly producing some noisy data. These noisy data points had to be eliminated to produce a smooth curve.

The material model used in LS Dyna also requires force-displacement data for compression, which is not provided by the tensile tests. This data thus had to be estimated. This estimation was either done by mirroring the tensile curve (Inner), extending the slope through the unloaded state into the compressive region (Outer, Foam) or adding a softening effect (Bladder). What method to use was decided by what gave the best fit to the experimental impact data.

Once the data was processed, LS Dyna included the fitted material parameters in the output files. These were then entered into the pre-processor so that the curve fit was not made again on every subsequent run.

3.1.2 DMA

The DMA testing began with the preparation of test specimens by extracting samples from each individual layer of the handball. Test specimen data is presented in Appendix A. When measuring the thickness, the Outer, Inner, and Bladder layers were uniformly thick, thus only a single measurement was taken of each sample. The Foam layer was irregular in thickness and thus determined as the mean value of three measurements. Additionally, the width of each sample was recorded. The length of the samples was measured by the Rheometer. The dimensions of each specimen can be found in Appendix A.

Additionally, as the volume of each sample was known with these measurements, they were also weighed to determine the density of each material layer.

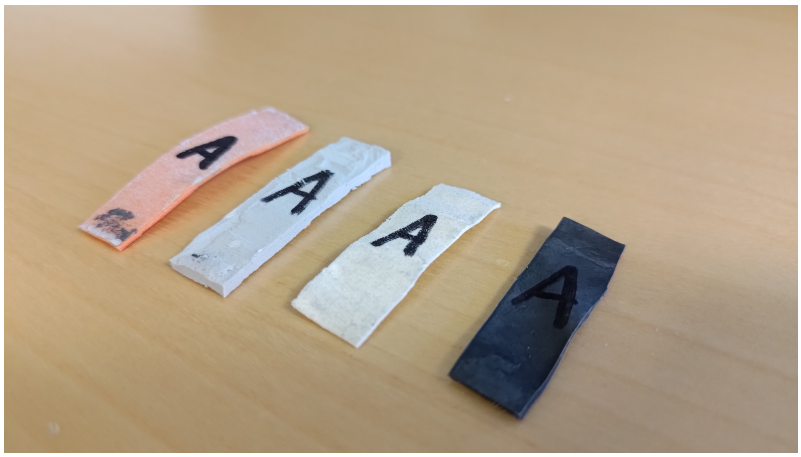

Figure 3.3: Samples used in the DMA

3.1.2.1 Experimental setup

To perform the DMA, an Anton Paar MCR 702 Rheometer was used. The test specimen was placed vertically and fastened into an Anton Paar solid rectangular fixture (SRF), cf. Figure 2.8. A slight axial pre-tension of 0.5-1.5 N was applied to straighten the samples. The results were monitored using the Anton Paar software RheoCompass.

Temperature was controlled by an Anton Paar EVU 20 evaporation unit. The unit was fed liquid nitrogen which cooled the specimen. The specimen was located inside a closed insulated chamber, the Anton Paar CTD 450 convection temperature device, which was only opened to mount the specimen and otherwise remains closed throughout the test.

3.1.2.2 Testing sequences performed

For each material layer, the first test conducted was an amplitude sweep, where the strain amplitude increased from 0.0001 % strain. During the amplitude sweep, storage modulus, loss modulus and loss factor for each strain amplitude were saved.

The behavior of these parameters were then used to select a strain amplitude within the linear viscoelastic region to be used in the coming frequency sweep.

In the subsequent frequency sweep, frequency and temperature were varied in increments. For each step in temperature, the frequency started at 20 Hz and ended at 0.1 Hz. The temperature started at −80 °C and increased in increments of 10 °C to the reference temperature T_{ref} of 20 °C. The strain amplitude is constant, 0.1 % for the Foam layer and 0.01 % for the Outer and Bladder layers, as determined from the amplitude sweep. Storage modulus, loss modulus and loss factor were extracted from the test.

3.1.2.3 Constructing the master curves

The raw DMA data is used to construct the master curves for each material layer. The data had to be post-processed before a fit into physical master curves was possible. This was due to some anomalous behavior at higher frequencies that caused nonphysical results, the cause of which was never identified. The frequency range of 0.1 Hz to 20 Hz had to be cut off after approximately 4 Hz. However, the frequency sweep steps through frequencies logarithmically, thus the majority of the data was still used (on average, 17 out of 24 data points per temperature).

Once the data was processed it was shifted into master curves, for a reference temperature T_{ref} of 20 °C, by the Python library `pyvisco` [42]. This library automatically determines shift factors and returns a complete master curve, given that the input data is physical.

3.1.2.4 Prony fit

The master curves are the input for constructing the Prony series, which is done according to [25]. Firstly, the storage modulus master curve was fitted to equation 2.19. The parameters determined in this fit are then modified to suit LS Dyna, which uses a slightly different formulation of equation 2.15, shown below

$$G_R(t) = \sum_{i=1}^{N} G_i e^{-\beta_i t} \tag{3.1}$$

LS Dyna uses decay constants β_i instead of relaxation times τ_i; the decay constants β_i are equal to $\frac{1}{\tau_i}$. Once modified and ensured to be in correct units, they are entered into the LS Dyna material cards, completing the implementation of viscoelasticity.

3.2 Physical experiments - Redbergslid IK

Tests were performed at Prioritet Serneke Arena (PSA) in Sports hall A together with Redbergslid IK during one of their training sessions. A triaxial load cell was used to measure all reaction forces, and high-speed cameras were used to capture the motion and deformation of the ball. A Dewesoft SIRIUS STG data acquisition system was used to trigger, synchronize and save measurements.

3.2.1 Load cell setup

The load cell was mounted to a steel frame rig, which in turn was mounted to a railing running along the side of the hall. The load cell model was a Denton 2358 triaxial load cell rated for 4.5 kN. An aluminum plate with a diameter 28.5 cm and weight of 2.59 kg was mounted on the load cell to provide an adequately large surface for the players to hit. On the backside, two 10 kg weights were mounted to reduce vibrations. A particle board was mounted around the load cell plate to stop any stray balls from impacting equipment or persons behind the load cell.

Figure 3.4: Back side of test rig and load cell setup

3.2.2 Camera setup

To enable video analysis two Dewesoft DS-CAM-GIGE-600 b/2 high-speed cameras were used to film the throws. Camera communication was handled by a Dewesoft CAM-BOX3 distribution system. The camera positions relative to the load cell are shown in Figure 3.5 and the distances in Table 3.1. For camera 1 (CAM 1) a 12 mm angle lens was used, and for camera 2 (CAM 2) a 11.5 mm angle lens. To allow tracking of the velocities and angles of the handball, backdrops were put in the

background of the filmed area. These were marked with yellow tape at distances of 0.2 m between every tape strip. Additionally, two crash test markers were placed in level on each backdrop.

After the test had been performed, the distances in Table 3.1 were measured using a tape measure. The distance was taken from the camera housing to corresponding backdrop surface or the center of the load cell.

Figure 3.5: Front side of test rig and camera setup

Table 3.1: Distances for camera setup

Between objects	Distance [m]
CAM 1 to Load cell	3.82 m
CAM 1 to Backdrop 1	5.04 m
CAM 2 to Load cell	1.81 m
CAM 2 to Backdrop 2	3.31 m

3.2.3 Test setup

The testing was conducted for three different impact scenarios. The players threw from approximate angles and exact impact angles were determined from the cameras.

- ≈90° head-on impact, no resin
- ≈90° head-on impact, resin applied
- ≈45° angled impact, resin applied

Data was acquired in 200 ms sequences, triggered by the normal force exceeding 300 N. Video and load cell data from 100 ms pre-trigger and 100 ms post-trigger was then recorded. The analog load cell signal was recorded at a frequency of 10 000 Hz using a full bridge configuration. The analog data was anti-alias filtered before digitization. Sensor excitation was set to 10 V. The cameras ran at their highest possible frame rate of 600 Hz with a resolution of 640x480.

3.2.4 Post-processing

To identify good throws for validation of the FE model, the force data was analyzed first. Every throw that generated a maximum absolute force in the Z-direction exceeding 1 kN was retained for further evaluation. Initially a preliminary video analysis was conducted, aimed to identify the impact point of the handball on the load cell. This was done by simply viewing all the footage. If a visually centered hit was observed, the throw was selected for more detailed video analysis.

For the detailed video analysis, the software TEMA was used. TEMA is a motion tracking and analysis software. With TEMA, a point could be placed on the ball and tracked during its motion. By using known reference distances, like the crash test markers, tape markings, and camera distances, a pixel can be related to real world distance. By also specifying the amount of frames per second, time and distance are correlated and TEMA outputs velocities of points traveling in the footage.

3.3 Handball model

Meshing and model creation was done in the ANSA pre-processor. The solver used was the LS Dyna R12.2.2 explicit with single-precision in MPP mode. The handball uses the mm-ms-kg unit system.

3.3.1 Property and element structure

The handball geometry is assumed to be a perfect sphere with a radius matching the ball's outer radius of 96.1 mm, which is also according to the IHF ball standard [15]. The handball was modeled with solid elements, grouped into four different properties representing the individual material layers. Each group was then subdivided into three through-thickness elements, except for the Foam material which had five through-thickness elements. The element division can be seen in Figure 3.6.

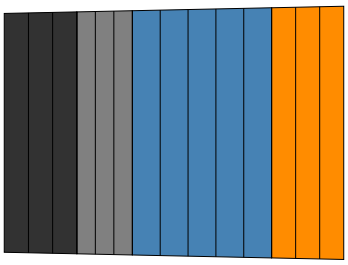

Figure 3.6: Cross-section of the handball showing element divisions. Materials from left to right: Bladder, Inner, Foam, Outer

The sphere was meshed mainly with hexahedral solid elements, with some additional pentahedrals added to accommodate the curvature of the ball. The element formulation used was "-2", which uses selective reduced integration. This integration scheme meant hourglassing was alleviated. The element formulation is also suited for the poor aspect ratio of the elements, reducing the risk of shear locking that might otherwise occur.

3.3.2 Material models

The material model used for all layers of the ball was material 77, `MAT_OGDEN_RUBBER`. This material model provides the Ogden hyperelastic rubber model according to [43] combined with a linear viscoelastic formulation according to [44].

The hyperelastic model was fitted by LS Dyna to force-displacement curves included as input, individual layer material parameters could then be extracted from the results after a first simulation run. Subsequent runs then instead used these material parameters as input, instead of performing the curve fit on every run.

The viscoelastic model was fitted externally in a Python script according to [25], from which an LS-Dyna .k file was generated and imported as an `INCLUDE`. This file conveniently also contained the force-displacement curves, ensuring that all material parameters were contained in one file. Note that the Inner material layer does not have a viscoelastic part.

3.3.3 Air pressure

A ball pressure of around 0.11 bar was what handball players from Redbergslid Idrottsklubb (RIK) identified as most commonly used in play, and is on the lower end of the allowed pressure range of 0.1-0.2 bar according to the handball rule-set. The pressure was measured with a manometer during an RIK training session. It should be noted that the pressure is not generally checked with a manometer by the players. The ball is pumped until it "feels right" for the players and this generally results in a pressure at or slightly above 0.1 bar.

Internal air pressure was modeled using the Airbag module, more specifically `AIRBAG_ADIABATIC_GAS_MODEL`. This model uses the Gamma Law Gas Equation of State to

compute the control volume pressure. The air pressure inside the ball was set to 0.11 bar gauge to an external atmospheric pressure of one standard atmosphere (101 325 Pa), along with a density ρ of 1.2 kg/m^3 and a heat capacity ratio γ of 1.4. A segment set was created on the inside surface mesh, which the airbag then acted upon. This was done as the airbag card required a set of segments to act upon, not nodes or elements.

3.3.4 Control cards

Dynamic relaxation is used by including `CONTROL_DYNAMIC_RELAXATION` and setting `IDRFLG=1` to deform the ball due to the air pressure inside it. The ball would be in an unbalanced state due to the air pressure if dynamic relaxation was not used. Mostly the default settings were used, but the dynamic relaxation factor `DRFCTR` was tuned to minimize the amount of iterations needed.

Other control cards used were the `CONTROL_ACCURACY` where the `OSU` and `INN` flags were set to 1 and 2 respectively. Both of these flags are recommend by LSTC when the material undergoes large deformations or rotations.

3.3.5 Contacts

The ball used the `CONTACT_AUTOMATIC_SURFACE_TO_SURFACE` card both in the case of contact to the aluminum wall and to the VIVA+ model. The coefficient of friction to the aluminum wall was set to 0.5. A viscous damping coefficient was set by the `VDC` flag to 30 %. The optional card `A` was used to set the soft constraint formulation to `SOFT=1`. All other parameters on this card were left as default.

3.3.6 Model setup - Handball and wall

When the model of the handball was created, a flat aluminum wall was meshed to emulate the aluminum plate mounted on the load cell. The rear of the plate was rigidly mounted and prevented from moving. Initial velocity of the ball was defined with `INITIAL_VELOCITY_GENERATION`, with input according to the velocity components measured in the TEMA point-tracking software for every impact scenario. The ball was positioned very close to the wall to minimize simulation time spent on rigid movement of the ball.

The resultant contact force components was then extracted by the database option `RCFORC` and the magnitude of the rigid body velocity by the `MATSUM` option. The contact force was divided into normal and transverse components, where the transverse component is defined as the vector magnitude of the two in-plane components of the aluminum wall. Three metrics were chosen to compare experimental results and simulated results. These were peak normal force, impact time and Coefficient of Restitution (COR, equation 3.2).

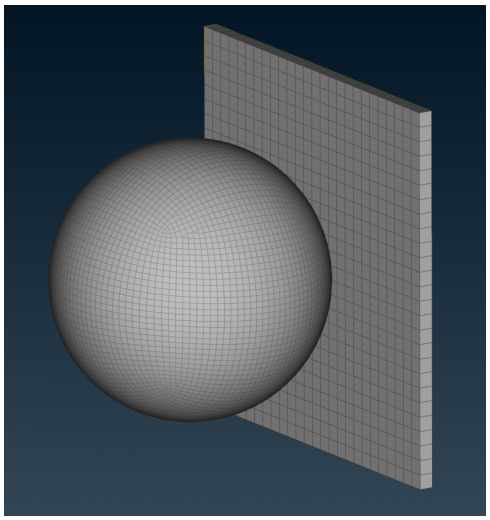

$$COR = \frac{v_{\text{out}}}{v_{\text{in}}} \tag{3.2}$$

Figure 3.7: Setup with ball and aluminum wall

3.4 Human Body Model in interaction with handball

FE simulations were used to determine the effect of simple protective head gear. These simulations were done in a model where the VIVA+ HBM and the FE model of the handball had been combined. To assess the risk of concussion, two primary impact scenarios were analyzed. Additionally, two supplementary scenarios were included to explore the influence of varying impact locations on the risk of concussion. The complete set of impact scenarios is illustrated in Figure 3.8.

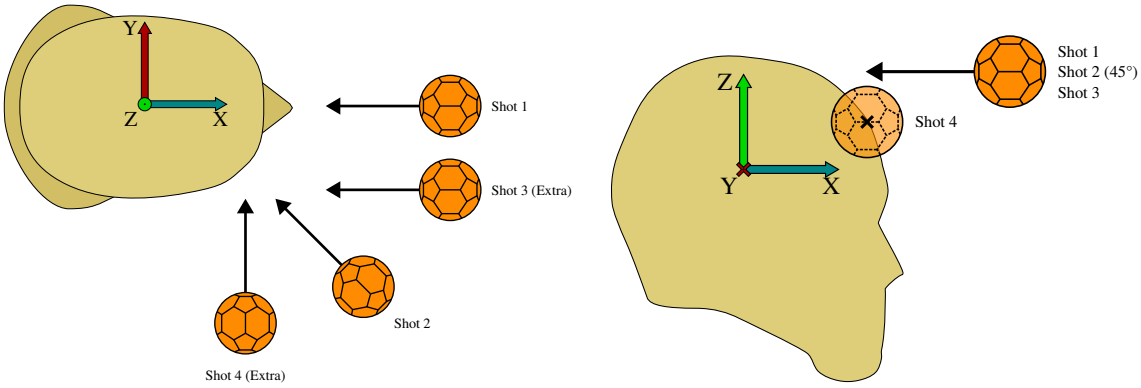

Figure 3.8: Impact scenarios for evaluation of simple protective head gear

3.4.1 Preparation of Human Body Model

A submodel of the VIVA+ HBM was used to study the impact between the handball and human head. Extraction of the submodel, which includes the head, neck and neck muscles, was done by Researcher Jobin John of the M2 Department. The element formulations, material definitions, internal contacts, and control cards were retained as defined in the original model and are documented in [29].

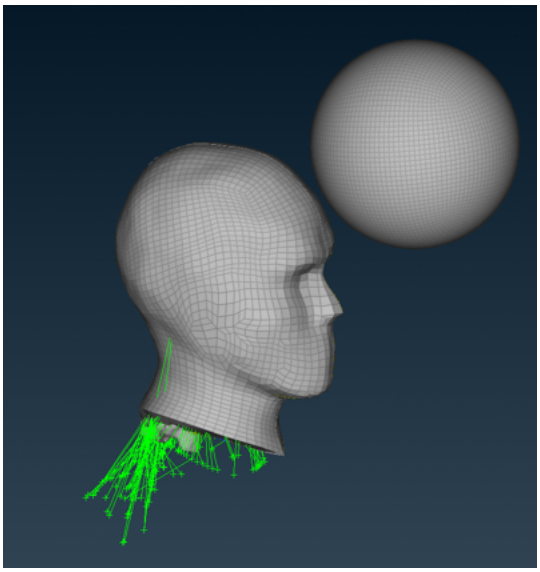

Figure 3.9: The submodel of the VIVA+ HBM, together with the handball

3.4.2 HBM + Handball setup

The submodel was imported into the ANSA pre-processor, where boundary conditions were applied to constrain the cut section. The face of the spine within the cutting region was fully constrained by fixing all translational and rotational degrees of freedom. Furthermore, translational movement in the Z-direction was restricted for nodes along the outer boundary of the cutting face.

Subsequently, the FE model of the handball, developed in Section 3.3, was imported as a *.k* file. The handball was then positioned and oriented using the `TRANSFORM` keyword. Table 3.2 defines the applied translations and rotations for each throw. These transformations were specified relative to a local coordinate system, designated `HE-Head-COG-Local`, which is located at node `1090000` and corresponds to the center of gravity of the head.

Shot nr.	dx [mm]	dy [mm]	dz [mm]	rx [°]	ry [°]	rz [°]
1	190.459	0	92.501	0	0	0
2	190.459	0	92.501	0	0	-45
3 (Extra)	180.459	-50	92.501	0	0	0
4 (Extra)	190.459	-10	72.501	0	0	-90

Table 3.2: Transformations relative to the head's center of gravity

Once the handball had been positioned accordingly, an initial velocity was applied using the `INITIAL_VELOCITY_GENERATION` keyword, with a magnitude of 30.556 m/s, corresponding to 110 km/h. The components of the initial velocity for each impact scenario are provided in Table 3.3.

Table 3.3: Initial velocities for different impact scenarios

Shot nr.	V_x [m/s]	V_y [m/s]	V_z [m/s]
1	-30.556	0	0
2	-21.606	21.606	0
3 (Extra)	-30.556	0	0
4 (Extra)	0	30.556	0

Additionally, a contact between the handball and the head of the submodel was defined using the `CONTACT_AUTOMATIC_SURFACE_TO_SURFACE` keyword, with the optional card `A` and soft constraint formulation enabled `SOFT=1`, while all other parameters were kept at their default settings. This model will from now on be referred to as VHHI (VIVA+ Head-Handball Impact) model.

3.4.3 Control cards

In simulations including the HBM in this study, the recommended control cards for the VIVA+ model were applied, as documented in [30]. Additionally , the control

cards described in Section 3.3.4 were also included. These simulations ran with a termination time of 25 ms and a time step of 0.3 µs.

3.4.4 Database option

Rotational velocities and accelerations of the head were recorded using the node `HE-Head-COG-Local` with `DATABASE_HISTORY_NODE_OPTION` enabled at a 0.01 ms sampling interval, generating an output containing the corresponding node data.

3.4.5 Adding protective gear

Based on the VHHI model developed in Section 3.4.2, an extended FE model was created incorporating a simplified protective headgear. The headgear was modeled by extruding a solid mesh with a total thickness of 10 mm, utilizing element formulation "-2". The mesh comprised two elements through the thickness, resulting in two layers, each 5 mm thick. All solid elements within a single layer were grouped into a distinct `PROPERTY`, yielding two additional property definitions, one for each helmet layer. Both properties were assigned a `MAT_057 LOW_DENSITY_VISCOUS_FOAM` material model.

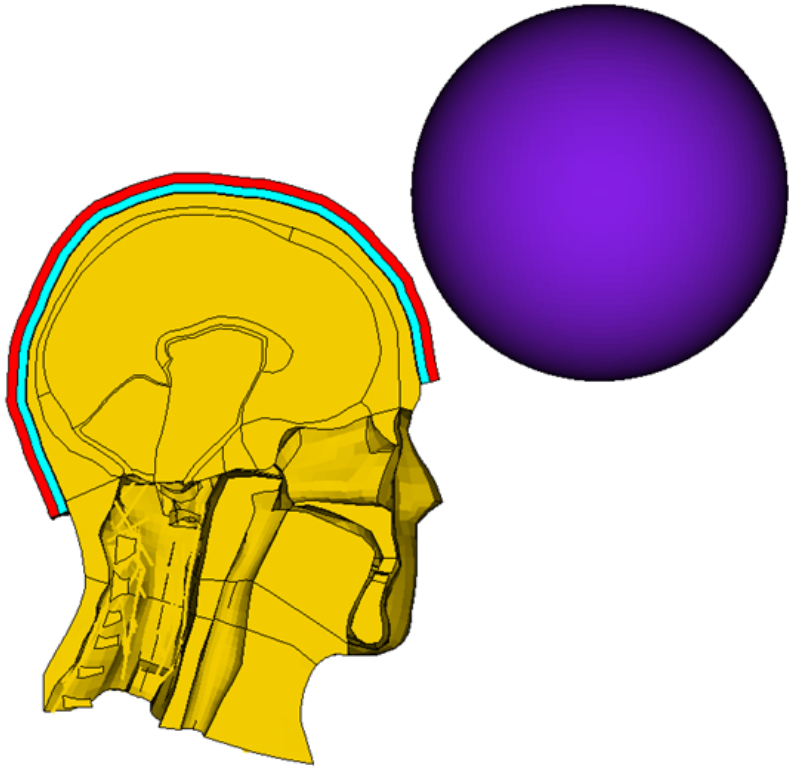

Figure 3.10: VIVA+ with the two sliding layers marked in red and cyan

To simulate a protective headgear with an internal sliding layer, multiple contacts were implemented. The following contacts were defined using the `CONTACT_`

`AUTOMATIC_SURFACE_TO_SURFACE` keyword. Optional card `A` was activated with the soft constraint formulation enabled, `SOFT=1`. Additionally, `PENCHK=2` was specified to correct for initial penetrations. The following contact interfaces were defined.

- Between the protective headgear and the head of the VIVA+ model.
- Between the two internal layers of the protective headgear.
- Between the protective headgear and the handball.

This FE model, which includes the protective headgear with an integrated sliding-layer mechanism, will be referred to as the VHSL (VIVA+ Headgear Sliding-Layer) model.

3.4.6 Testing sequences

Three main testing sequences were performed, each applied only to impact scenarios one and two. These are outlined below. Additionally, impact scenarios three and four were simulated in the VHHI model, using static and dynamic coefficients of friction set to 0.7.

- **Friction Sweep – VHHI model:** For the VHHI model, a friction sweep was conducted using static and dynamic coefficients of friction ranging from 0.1 to 1.0 in increments of 0.1.
- **Stiffness Variation – VHSL model:** For the VSHL model, a parametric study was performed on the Young's modulus of the foam in both sliding layers. Simulations were carried out for values of 2, 4, 6, 8, 10, and 20 MPa. The following friction coefficients were defined and held constant throughout all simulations:
  - Helmet-to-head: 0.6
  - Helmet-to-ball: 0.8
  - Between sliding layers: 0.2
- **Internal Friction Sweep – VHSL model:** For the VSHL model, a sweep of the internal friction coefficient between the sliding layers was conducted. The coefficient was varied from 0.1 to 0.6 in increments of 0.1. The following parameters were held constant throughout these simulations:
  - Young's modulus: 2 MPa
  - Helmet-to-head: 0.6
  - Helmet-to-ball: 0.8

3.4.7 Post-processing and risk assessment

To assess the risk of concussion, the DYNASAUR Python package was employed [45]. The DAMAGE metric was computed from rotational motion data extracted from the output for node `1090000`, identified as `HE-Head-COG-Local`. Based on the calculated DAMAGE value, DYNASAUR estimated head injury risk using AIS risk functions. In this study, AIS 2 levels were considered, as they correspond to mild traumatic brain injuries, such as concussions.

4
Results

This section uses a color coding scheme when presenting results relating to the individual materials of the handball. The scheme is defined as below.

- Outer
- Foam
- Inner
- Bladder

The first section presents the raw data from material tests. The second section presents the material data as adapted by the handball model. Thirdly, force and velocity measurements from experiments and simulations are presented for each impact scenario between the handball and wall. Lastly, the impact scenarios between HBM and handball are presented.

All materials are plotted in the same figure if possible. Otherwise a split into stiffer materials (outer, inner) and softer materials (foam, bladder) may be done to increase readability.

4.1 Material testing

4.1.1 Tensile test

Results of the tensile tests are presented as graphs with change in length to force applied.

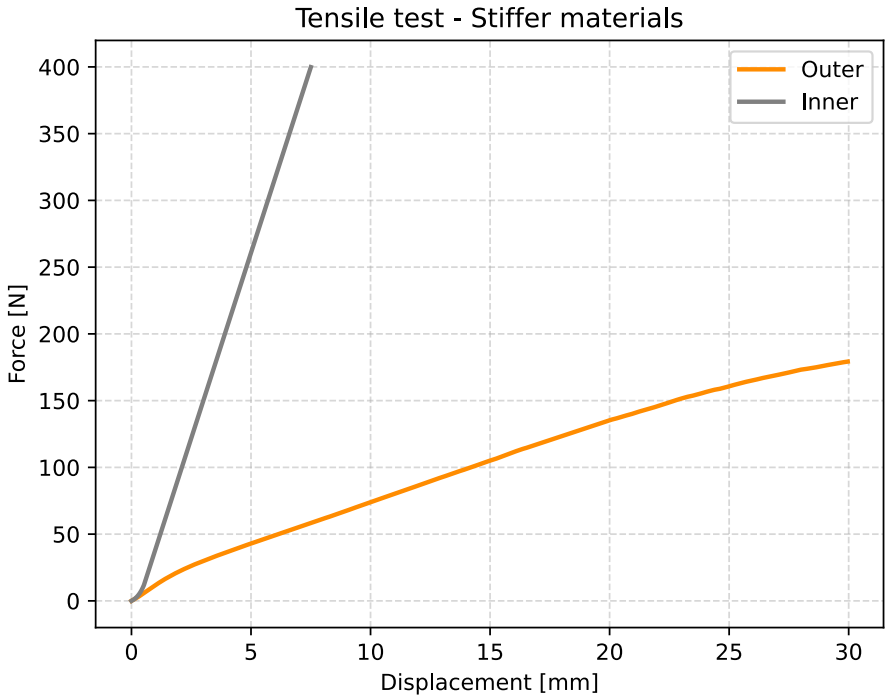

Figure 4.1: Results of tensile test, outer and inner materials

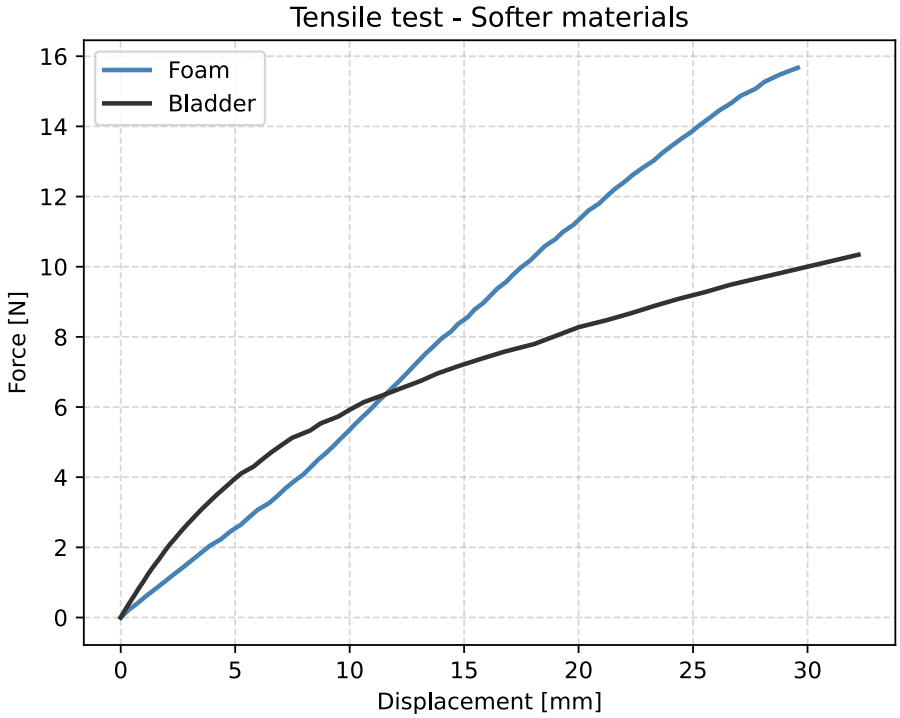

Figure 4.2: Results of tensile test, foam and bladder materials

4.1.2 DMA

Results of the DMA are presented as graphs with frequency to storage and loss modulus.

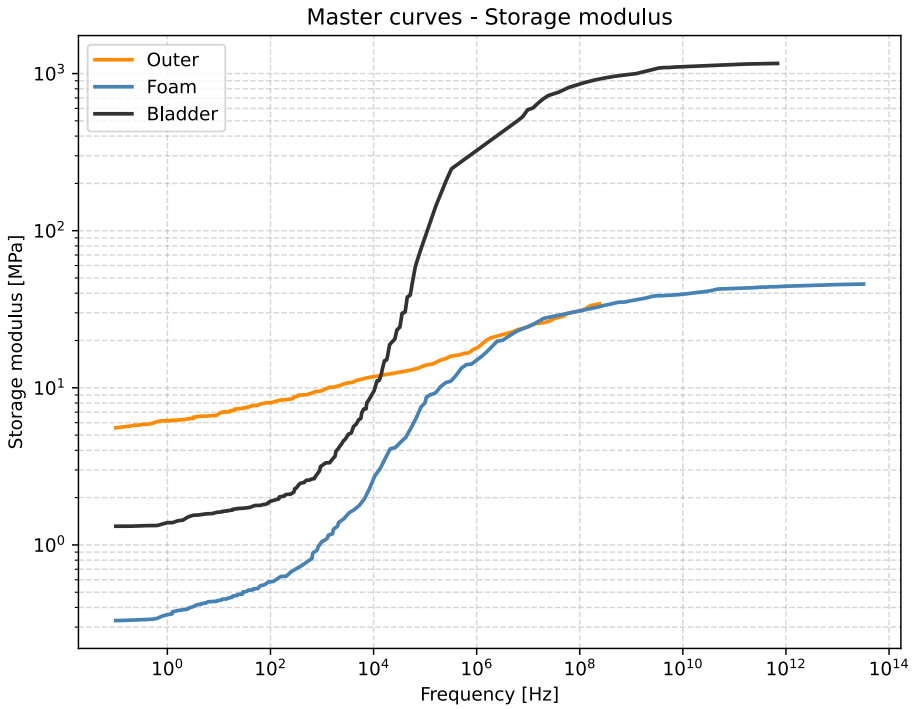

Figure 4.3: Storage modulus master curves for all viscoelastic materials

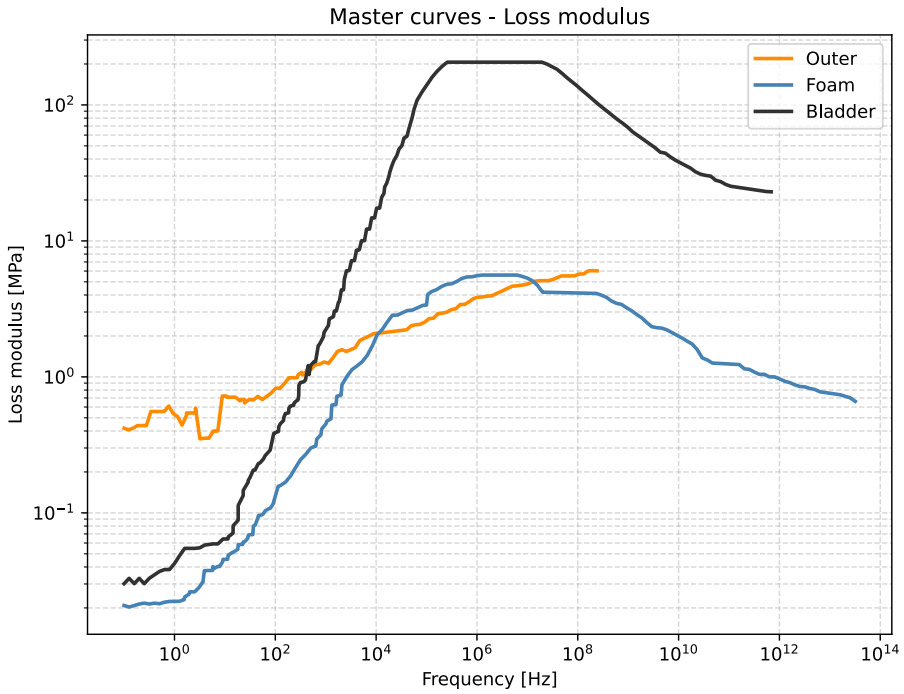

Figure 4.4: Loss modulus master curves for all viscoelastic materials

4.2 Handball model

4.2.1 Elasticity

Stress-stretch curves for determining the elastic response of each material are presented below.

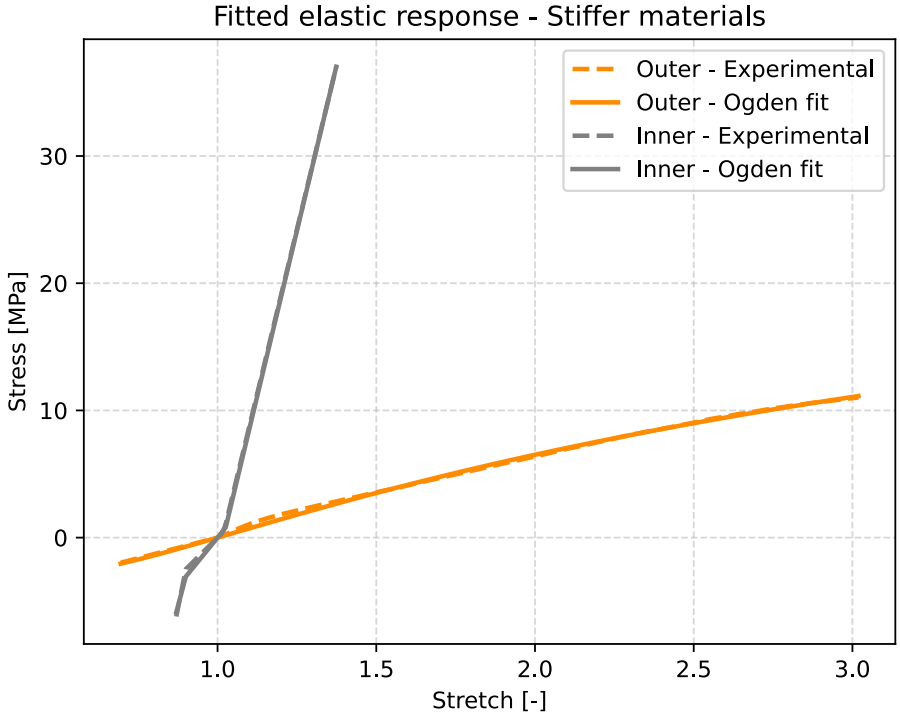

Figure 4.5: Stress-stretch curve, outer and inner materials

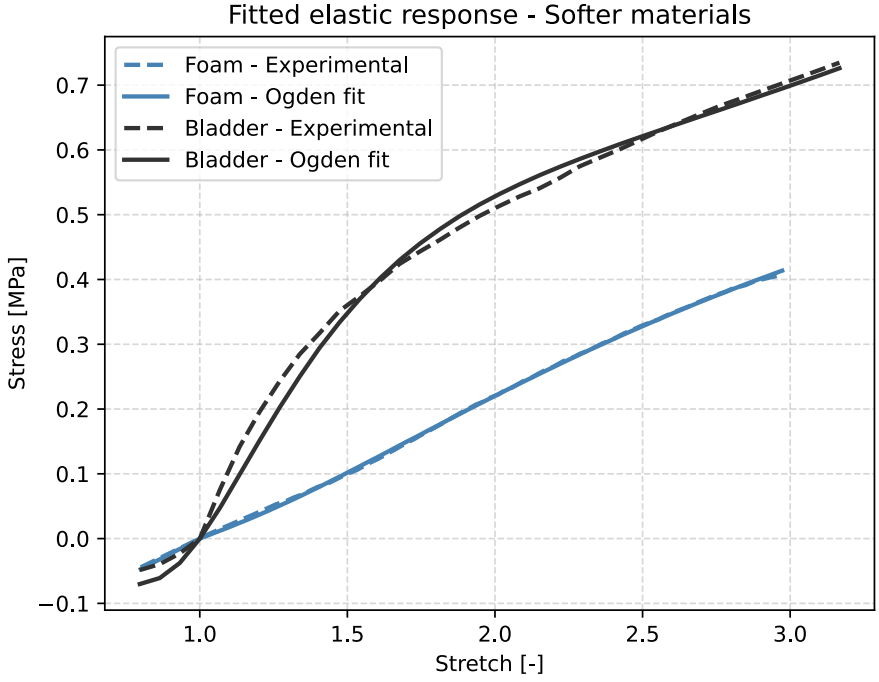

Figure 4.6: Stress-stretch curve, foam and bladder materials

Material parameters resulting from the elastic data are presented in table 4.1. These are the actual values entered into the LS-Dyna material model.

Table 4.1: Ogden hyperelastic parameters, units for μ in GPa

Material	μ_1	μ_2	μ_3	μ_4	μ_5
	α_1	α_2	α_3	α_4	α_5
Outer	0.0266	-0.2982	-	-	-
	1.0979	0.0819	-	-	-
Foam	0.0050	0.0106	-0.0024	-	-
	0.5318	-0.5254	-1.2558	-	-
Inner	-1.7669	1.5249	-0.3308	-	-
	-1.5816	-2.8511	-4.7493	-	-
Bladder	-0.0070	0.0049	-0.0014	7.316e-5	-3.606e-9
	-1.2735	-2.9617	-4.5563	-6.7260	-14.5404

4.2.2 Viscoelasticity

Point-wise storage modulus DMA data and fitted Prony series for determining the viscous response of each material are presented below.

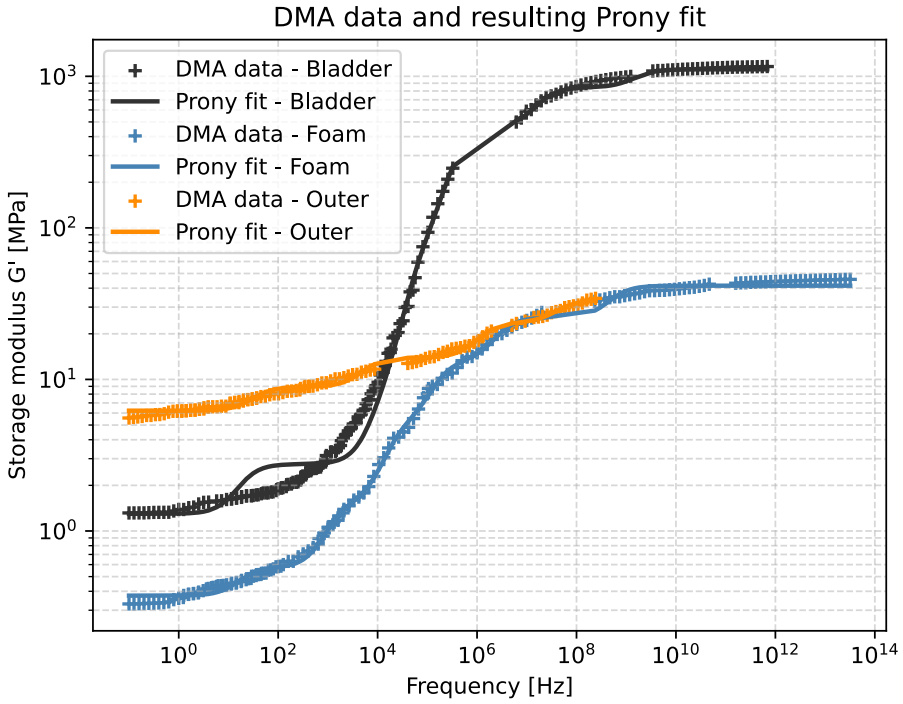

Figure 4.7: Prony fit in time domain, outer skin

Material parameters resulting from the viscoelastic data are presented in table 4.2. These are the actual values entered into the LS-Dyna material model.

Table 4.2: Viscoelastic parameters, units for G in GPa and β in 1/ms

Material	G_1	G_2	G_3	G_4	G_5	G_6
	β_1	β_2	β_3	β_4	β_5	β_6
Outer	2.7217e-3	9.7925e-3	5.0166e-3	9.5239e-3	-	-
	3.2978e-2	1.1200e3	5.2908e0	4.1567e4	-	-
Foam	2.0054e-4	9.7792e-4	3.7288e-3	8.0025e-3	1.2311e-2	1.5948e-2
	1.7617e-2	1.1229e0	1.7864e1	1.4820e2	2.5879e3	4.9966e5
Bladder	1.4653e-3	3.9722e-3	7.0888e-2	3.9165e-1	3.7645e-1	2.6640e-1
	1.7987e-2	9.7279e0	5.8521e1	3.5477e2	1.7389e4	1.5115e6

4.2.3 Additional material parameters

Material parameters for density, Poisson ratio and the thickness of each layer are presented in table 4.3. These are the actual values entered into the LS-Dyna material model.

Table 4.3: Parameters density ρ, Poisson ratio ν and layer thickness t, units for ρ in kg/mm^3 and t in mm

Material	ρ	ν	t
Outer	5.64e-7	0.49	1.3
Foam	2.49e-7	0.49	2.5
Inner	8.57e-7	0.49	1.0
Bladder	9.50e-7	0.499	1.3

4.3 Impact scenarios - Handball and wall

Inbound and outbound velocities for all impact scenarios are presented in Table 4.4. These are averaged velocities before and after impact from the point-tracking software TEMA. High speed camera footage reported all impact times as approximately 10 ms.

Table 4.4: Average inbound and outbound velocities (unsigned), and COR, from the TEMA point-tracking for all shots

Throw nr.	V_Z^{in} [m/s]	V_Z^{out} [m/s]	V_Y^{in} [m/s]	V_Y^{out} [m/s]	V_X^{in} [m/s]	V_X^{out} [m/s]	V_{total}^{in} [m/s]	V_{total}^{out} [m/s]	COR
No resin, head-on 1	22.450	10.773	2.262	2.622	-	-	22.591	11.136	0.493
No resin, head-on 2	24.907	11.798	3.500	0.105	-	-	25.152	11.798	0.469
No resin, head-on 3	25.615	12.283	3.950	3.005	-	-	25.926	12.711	0.490
Resin, head-on 1	27.185	12.891	2.731	2.158	-	-	27.393	13.076	0.477
Resin, angled 1	19.845	10.560	4.598	2.832	8.757	3.830	22.196	11.70	0.527
Resin, angled 2	21.179	11.578	3.015	0.195	10.012	3.762	24.175	10.850	0.449

A quick reference to the impact scenario and coordinate system definitions is presented Figure 4.8. In the coming figures, results marked "Experimental" represent recorded throws by RIK players during the physical tests. Results marked "Simulation" represent simulations with inbound velocities from Table 4.4 as initial conditions. The data has not been filtered.

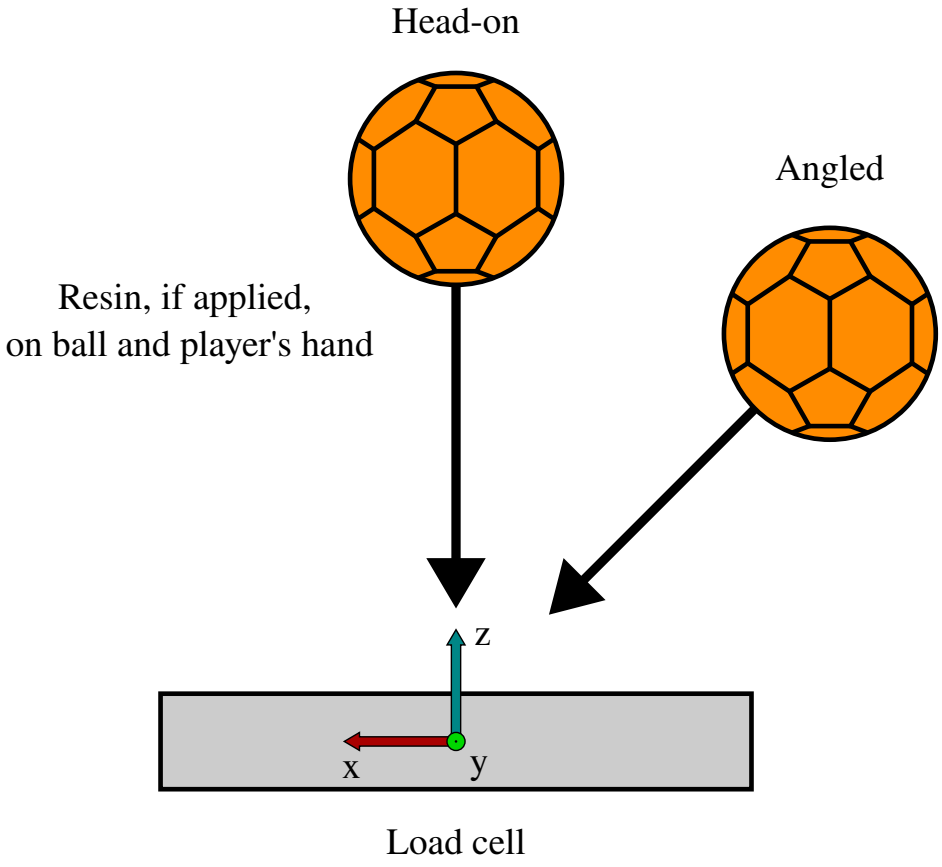

Figure 4.8: Quick reference of definitions for the impact scenarios presented in the coming figures. Viewed from above the load cell

4.3.1 No resin, head-on 1

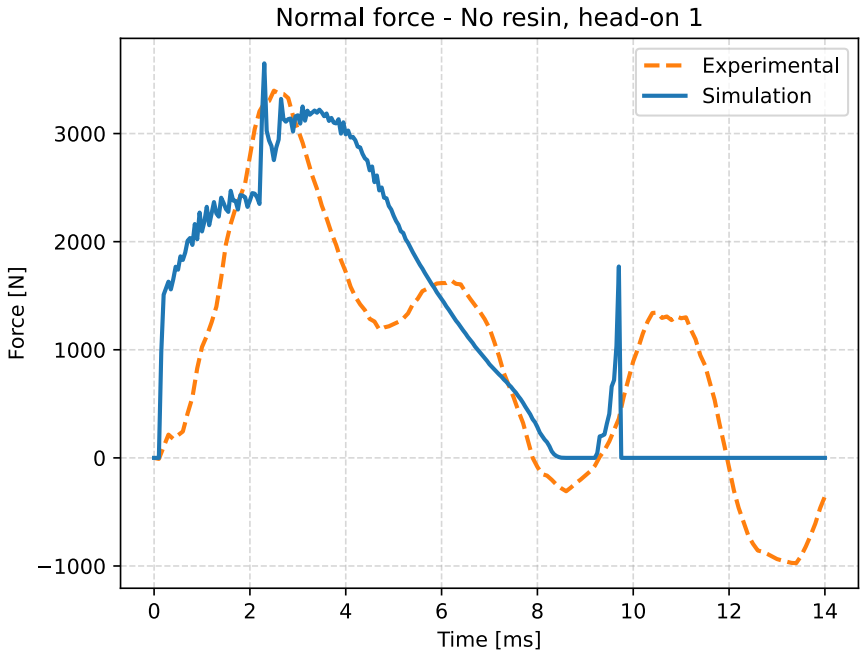

Figure 4.9: Normal force over time for shot "No resin, head-on 1"

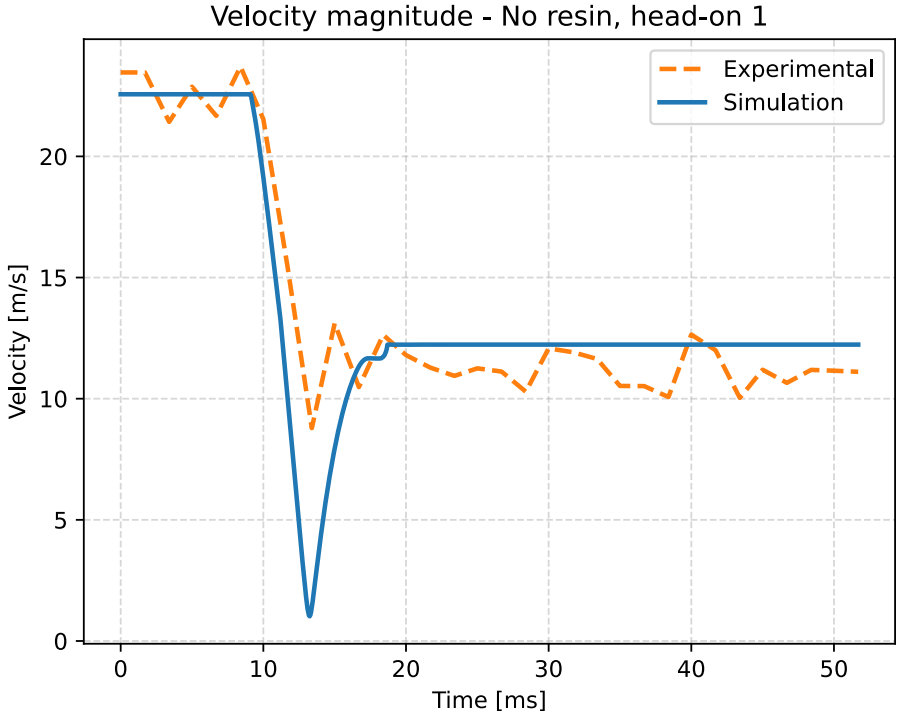

Figure 4.10: Magnitude of velocity over time for shot "No resin, head-on 1"

4.3.2 No resin, head-on 2

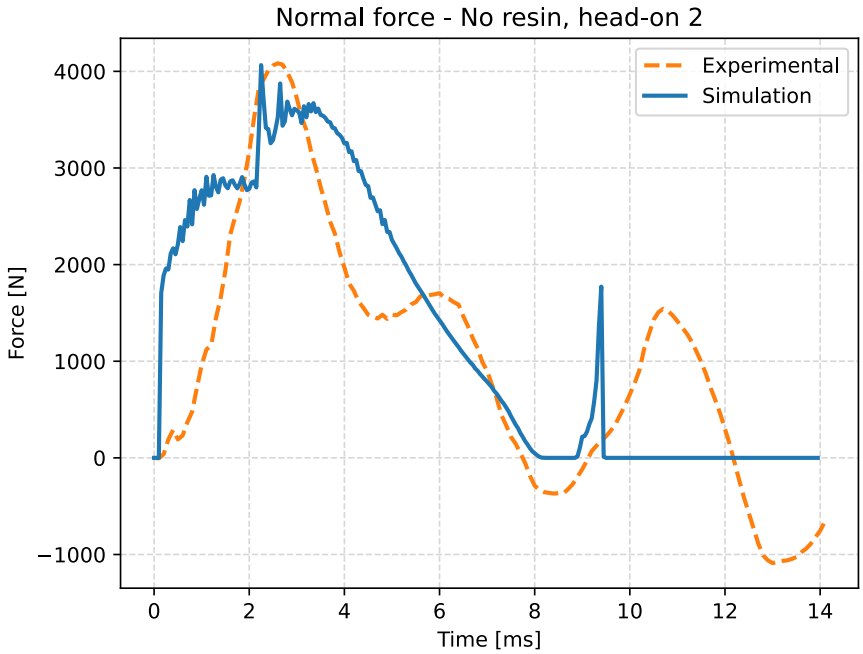

Figure 4.11: Normal force over time for shot "No resin, head-on 2"

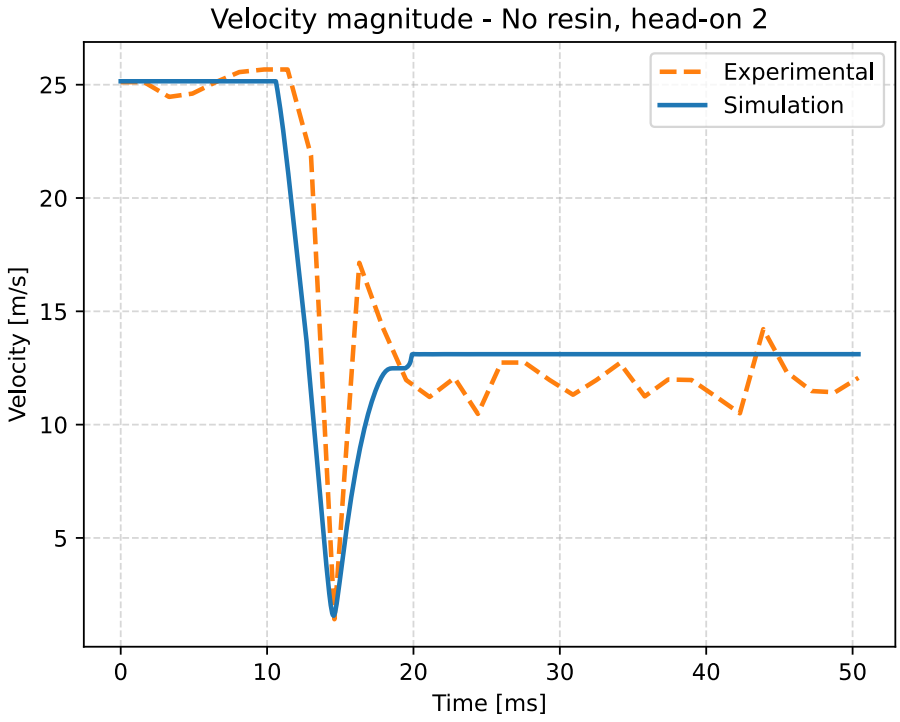

Figure 4.12: Magnitude of velocity over time for shot "No resin, head-on 2".

4.3.3 No resin, head-on 3

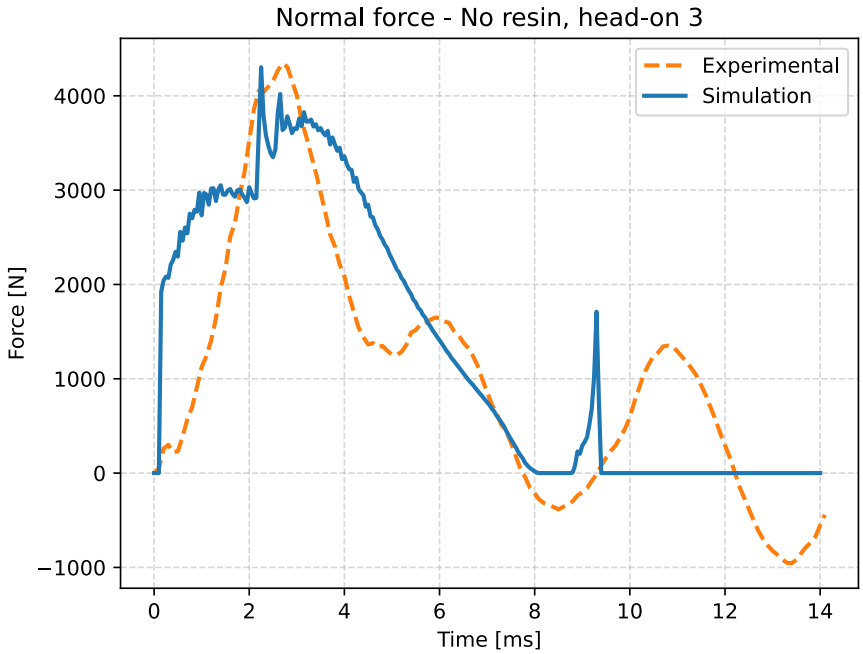

Figure 4.13: Normal force over time for shot "No resin, head-on 3"

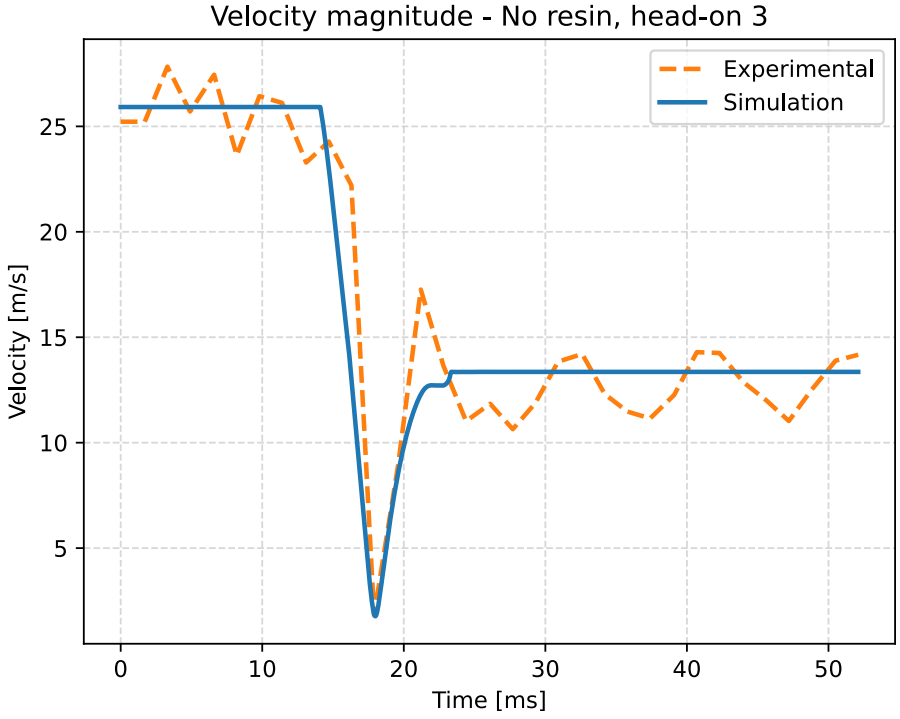

Figure 4.14: Magnitude of velocity over time for shot "No resin, head-on 3"

4.3.4 Resin, head-on 1

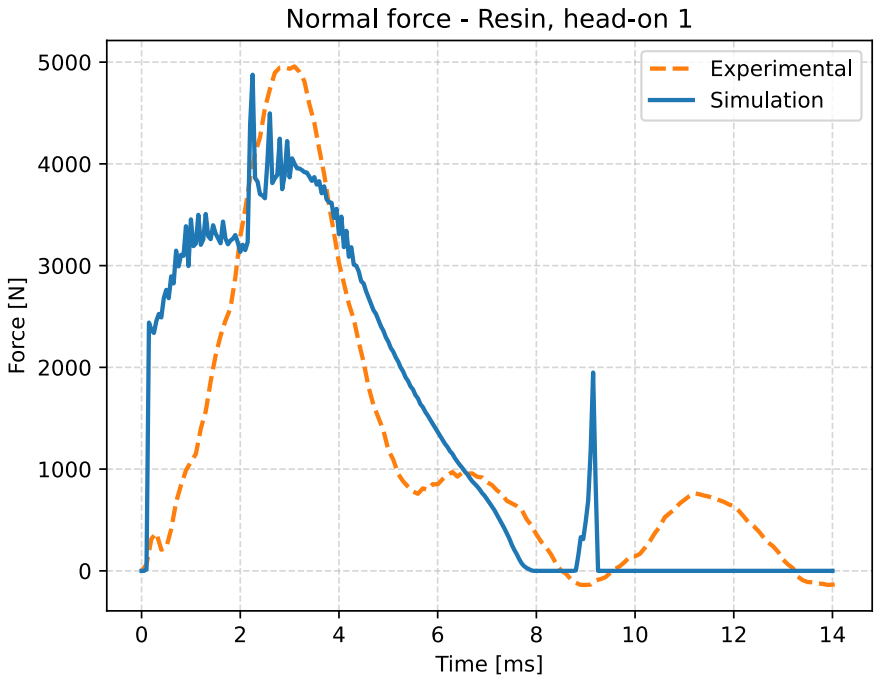

Figure 4.15: Normal force over time for shot "Resin, head-on 1"

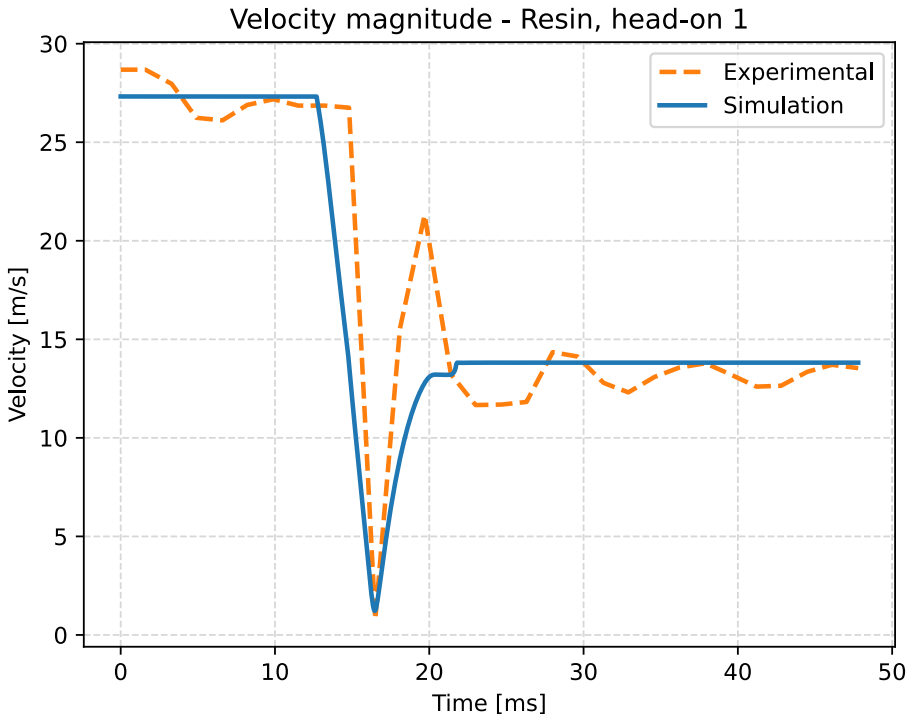

Figure 4.16: Magnitude of velocity over time for shot "Resin, head-on 1"

4.3.5 Resin, angled 1

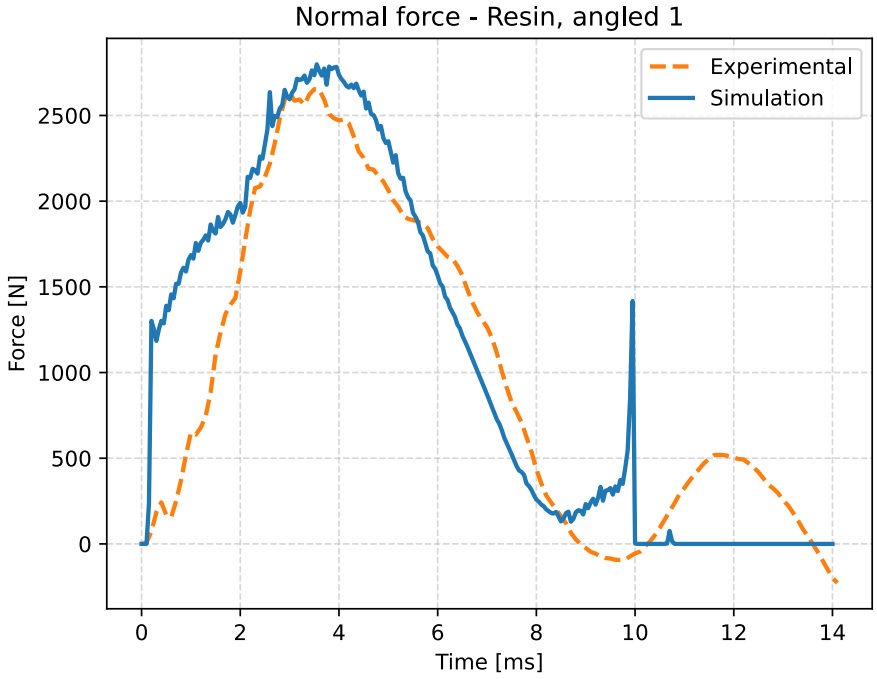

Figure 4.17: Normal force over time for shot "Resin, angled 1"

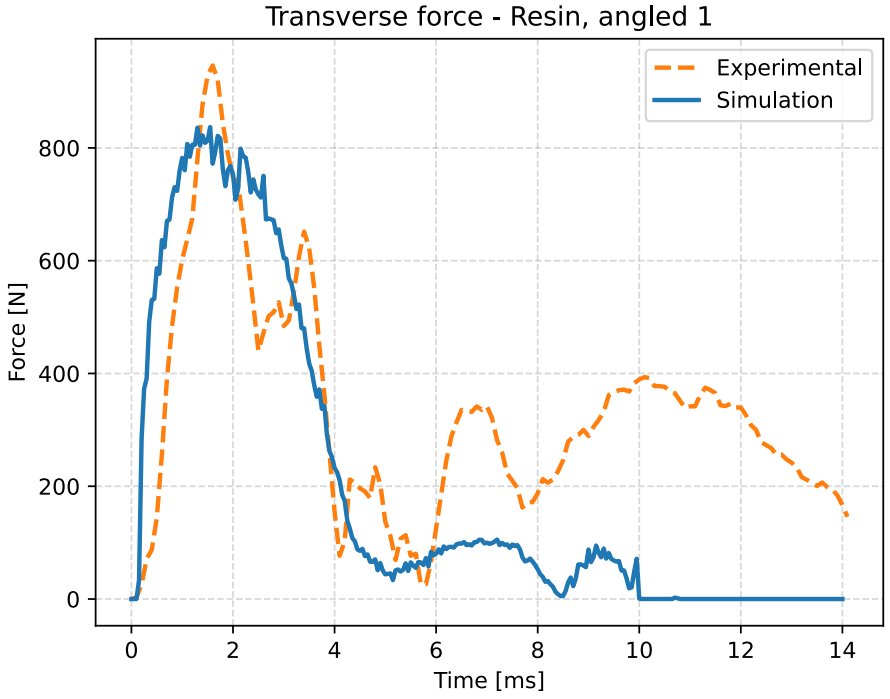

Figure 4.18: Transverse force over time for shot "Resin, angled 1"

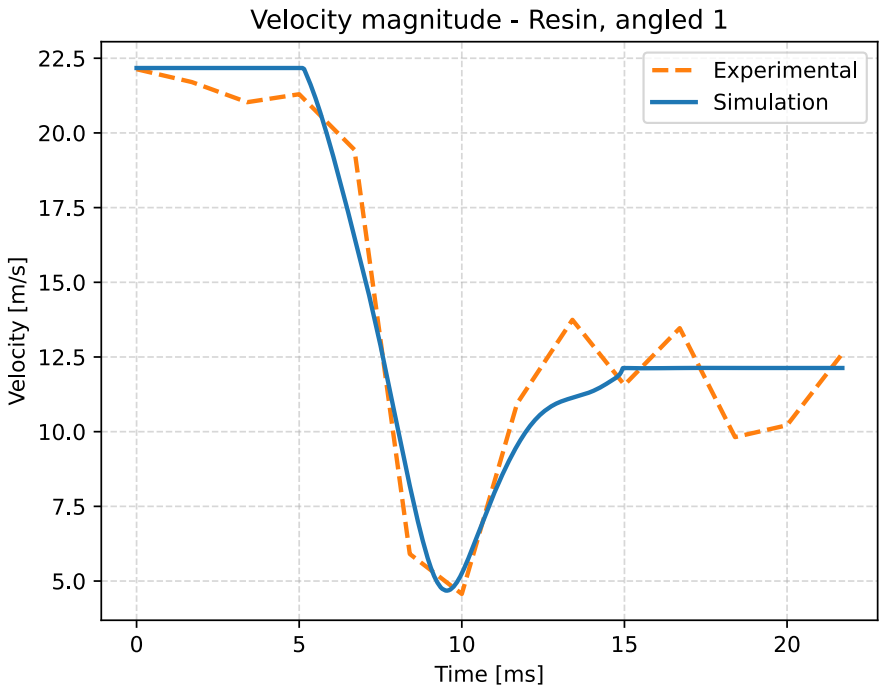

Figure 4.19: Magnitude of velocity over time for shot "Resin, angled 1"

4.3.6 Resin, angled 2

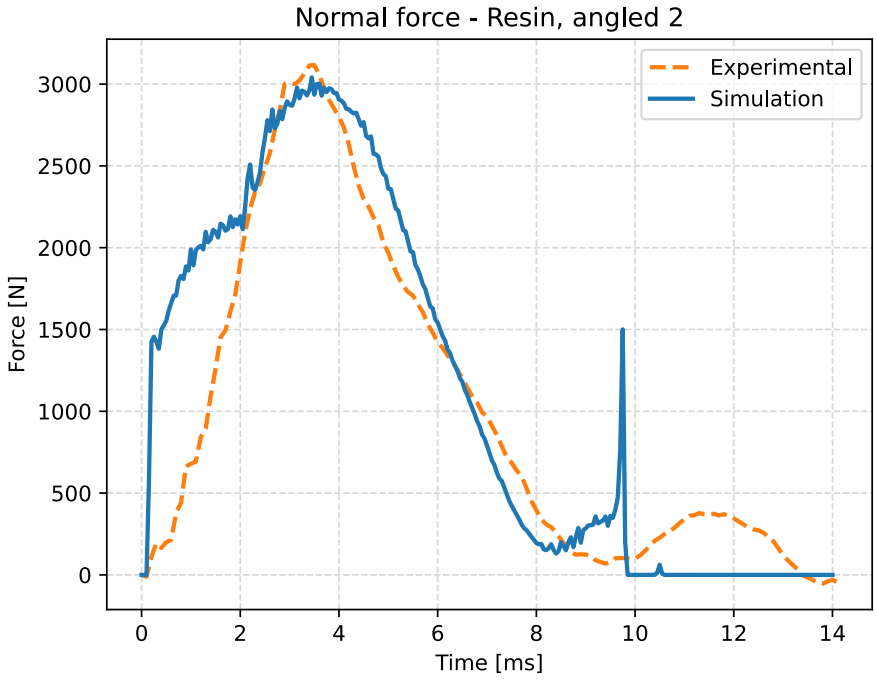

Figure 4.20: Normal force over time for shot "Resin, angled 2"

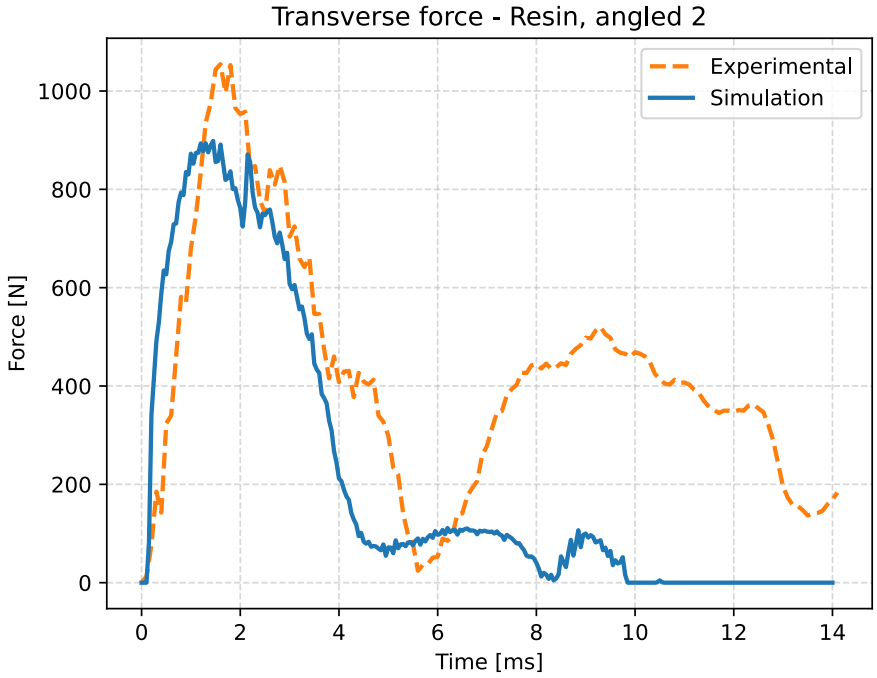

Figure 4.21: Transverse force over time for shot "Resin, angled 2"

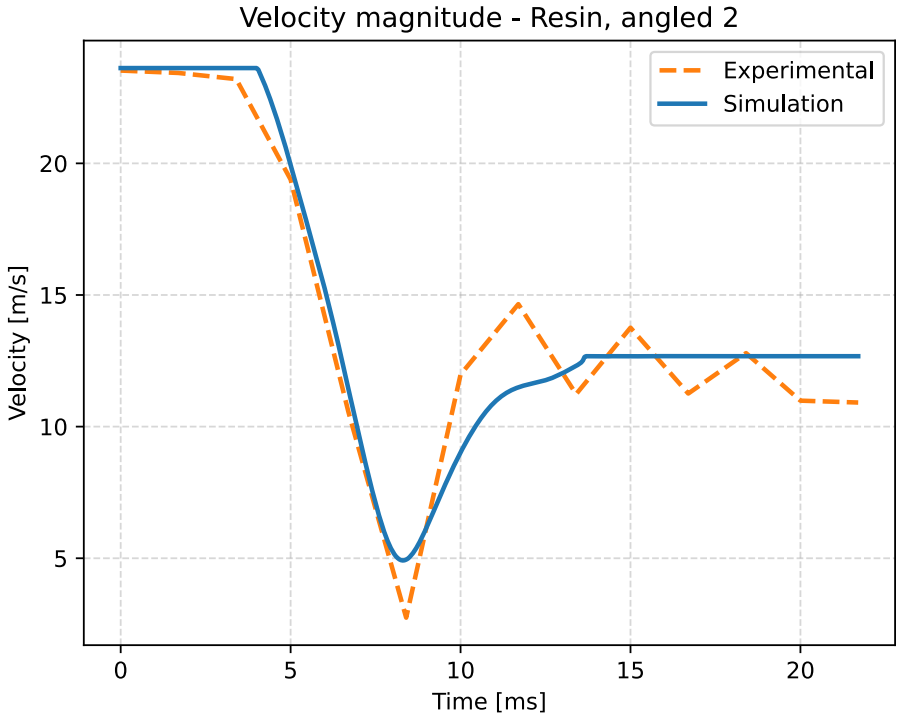

Figure 4.22: Magnitude of velocity over time for shot "Resin, angled 2"

Lastly, a collection of metrics to be evaluated from all impact scenarios, experimental and simulated, along with their percentage difference. The experimental impact time comes from the high speed camera footage.

Table 4.5: Comparison of all impact scenarios

Impact scenario	Peak force [kN]			Impact time [ms]			COR [-]		
	Exp.	Sim.	Diff. %	Exp.	Sim.	Diff. %	Exp.	Sim.	Diff. %
No resin, head-on 1	3.40	3.65	7.09	10	9.80	2.02	0.493	0.542	9.47
No resin, head-on 2	4.08	4.06	0.49	10	9.50	5.13	0.469	0.521	10.50
No resin, head-on 3	4.34	4.30	0.93	10	9.44	5.76	0.490	0.515	4.97
Resin, head-on 1	4.96	4.88	1.63	10	9.30	7.25	0.477	0.506	5.90
Resin, angled 1	2.65	2.80	5.50	10	10.03	0.30	0.527	0.547	3.72
Resin, angled 2	3.12	3.04	2.60	10	9.88	1.21	0.449	0.537	17.85

4.4 Impact scenarios - Handball and HBM

This section pertains to shots one, two, three, and four, as illustrated in Figure 3.8. The abbreviations VHHI and VHSL refers to the different FE models developed in Section 3.4.2 and 3.4.5 respectively.

An added mass of 9.3449×10^{-5} kg was introduced during the simulations for both VHHI and VHSL models. The physical mass of the VHHI and VHSL models were 5.9191 kg and 5.9947 kg, yielding a percentage increase of 0.0015788 and 0.0015589 % respectively.

4.4.1 Frictions impact on risk of concussions

Risk of injury based on AIS 2 risk curves, from the DAMAGE injury criteria, for varying friction are presented below.

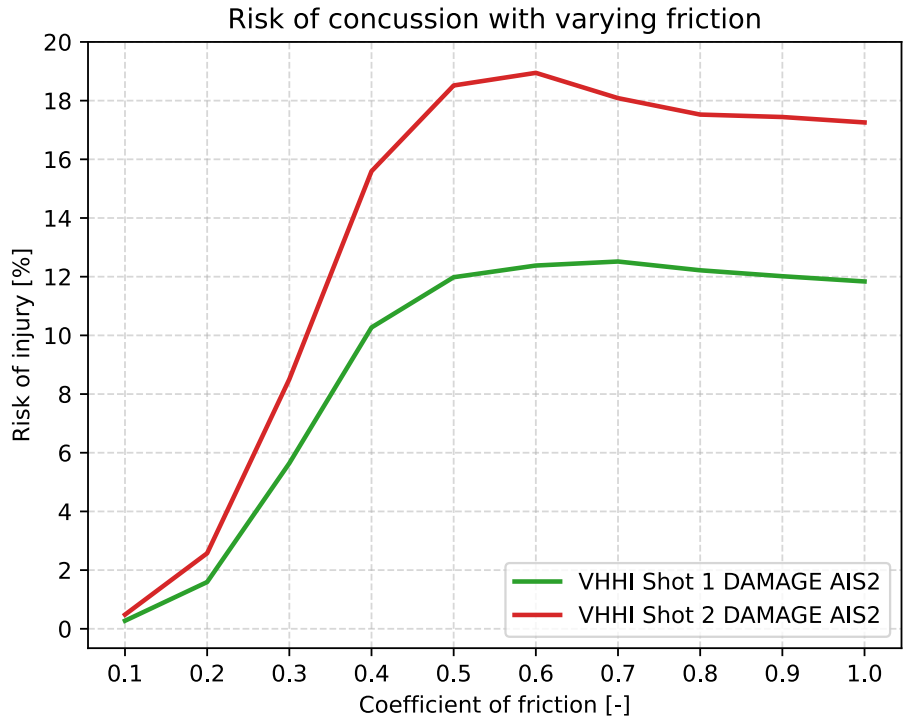

Figure 4.23: Risk of injury for varying coefficient of friction between the handball and VIVA+ model

4.4.2 Damping materials impact on risk of concussion

Risk of injury based on AIS 2 risk curves, from the DAMAGE injury criteria, for varying stiffness of the foam in the VHSL model are presented below.

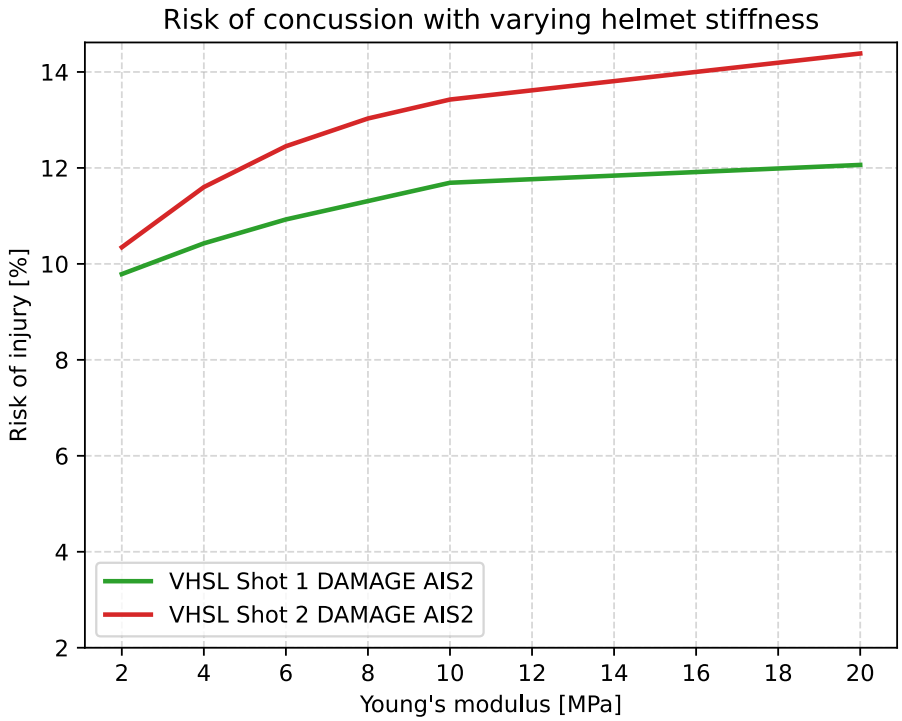

Figure 4.24: Risk of injury for varying stiffness of damping material

4.4.3 Sliding layer helmet implemented

Risk of injury based on AIS 2 risk curves, from the DAMAGE injury criteria, for varying friction between the sliding layers of VHSL model are presented below.

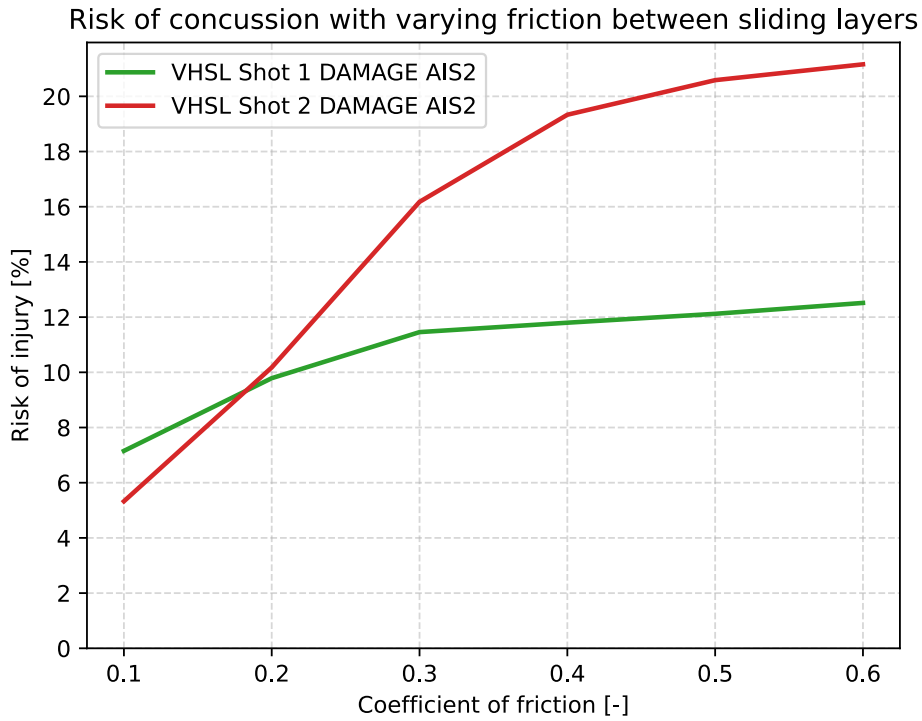

Figure 4.25: Risk of injury for varying coefficient of friction between sliding layers

4.4.4 Additional shots

Table 4.6 presents the AIS 2 risk values, as calculated using the DAMAGE injury criterion, for impacts three and four on the VHHI model.

Shot nr.	**DAMAGE (AIS 2)** [%]
3 (Extra)	21.3936626
4 (Extra)	34.8549238

Table 4.6: Risk of injury for two additional impact scenarios

4.4.5 Deformation view

Figure 4.26 to 4.29 show the deformations occurring during an impact. The impact scenarios shown in the figures are in order one, two, three and four.

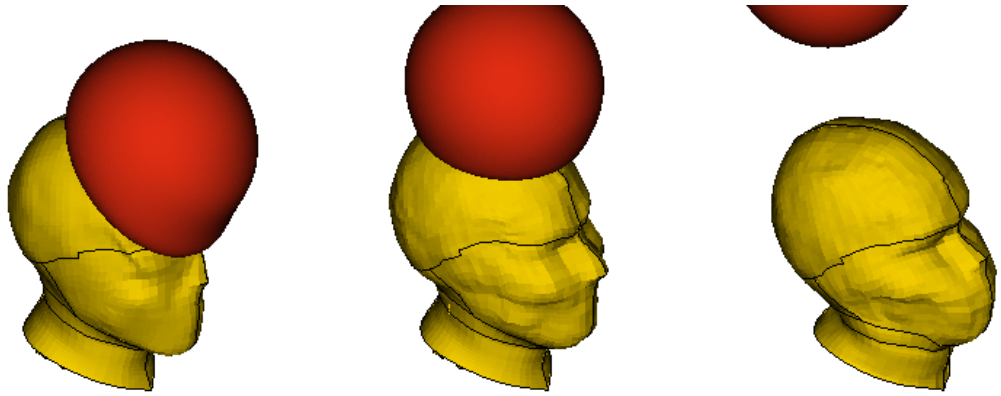

Figure 4.26: Head deformation and displacement during simulation of impact scenario one. Images at 5 ms, 12 ms and 20 ms

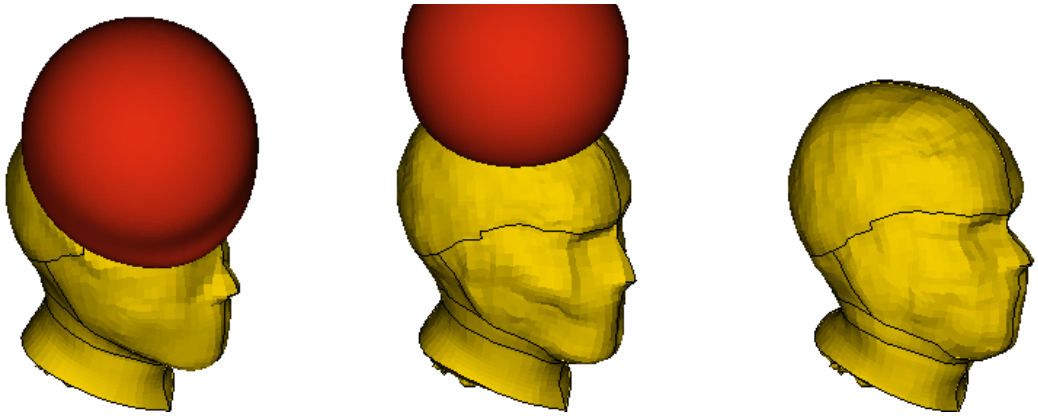

Figure 4.27: Head deformation and displacement during simulation of impact scenario two. Images at 5 ms, 12 ms and 20 ms

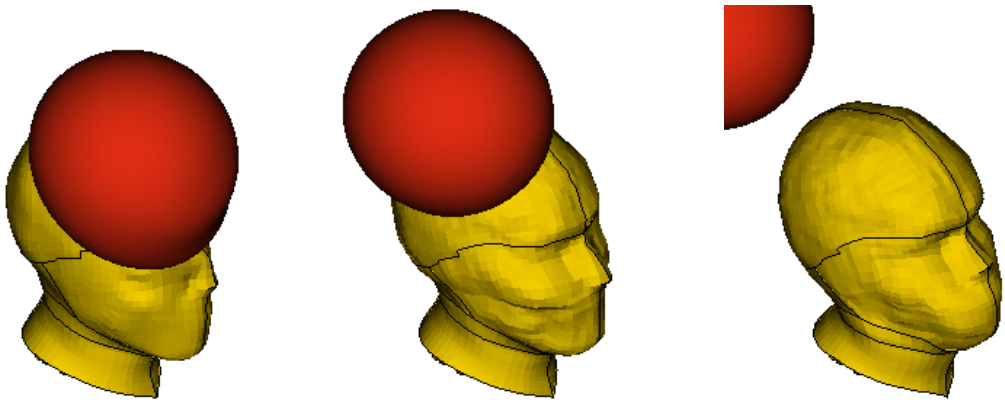

Figure 4.28: Head deformation and displacement during simulation of impact scenario three. Images at 5 ms, 12 ms and 20 ms

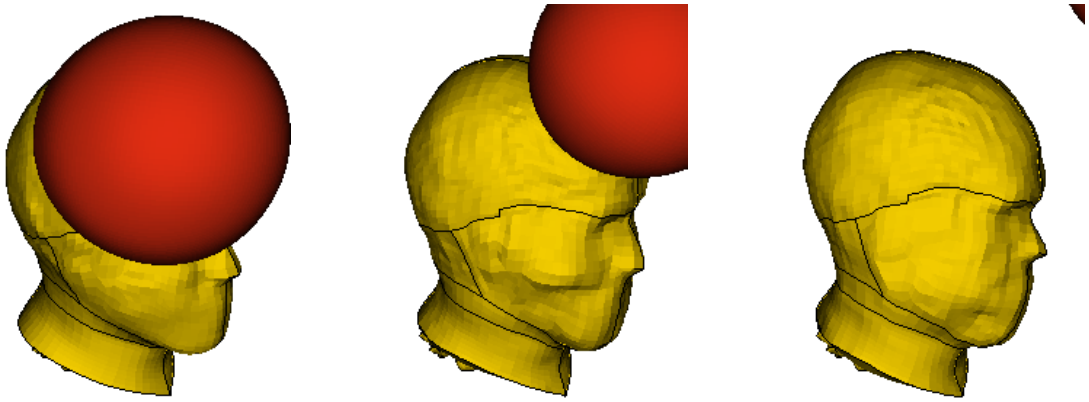

Figure 4.29: Head deformation and displacement during simulation of impact scenario four. Images at 5 ms, 12 ms and 20 ms

5
Discussion

5.1 Material testing

The material testing found the ball to consist of four very different materials. As seen in the storage and loss moduli (Figure 4.3 and 4.4), the bladder and foam material display the largest variation in moduli for high frequencies, contributing significantly to the damping effects of the ball. Thus the choice of a more advanced material model, like the Ogden Hyperelastic model combined with linear viscoelasticity, seems to be a necessity in modeling the handball.

In regards to the exact material model choice, it is possible that more suitable models exist. The Ogden model was chosen as it was powerful yet simple to adapt, with the possibility to add or remove terms as needed. But due to the very different nature of the materials, better results might be achieved by using different material models for each material layer. LS Dyna contains textile and foam material models that could be better suited for these materials, but using these require different input data and thus more material testing. Material testing is time-consuming, which was the main limiting factor leading to the choice of only one model. Even so, the handball model does manage to match the real ball well in all impact scenarios.

5.1.1 Exclusion of the Inner layer viscoelasticity

The Inner layer is noticeably absent from the viscoelastic material testing data. While a sample was created for the Inner layer, it was never tested in the DMA. The DMA ran in the order of priority: Outer, Foam, Bladder, Inner. The liquid nitrogen ran out after testing the Bladder layer which meant that the Inner layer could not be tested for viscoelasticity. It was assumed that the rubber-like materials of the Outer, Foam and Bladder layers would contain more significant viscoelastic properties, hence the order of testing priority. However, this was never confirmed and remains as a possible error source.

5.1.2 Non-linear viscoelasticity

As seen in Figure A.1, the storage and loss moduli are not constant for all strain amplitudes, they decrease for increased strain amplitudes. This is known as the Payne effect, which requires non-linear viscoelasticity to capture [16, ch.8]. To model this, material testing also needs to be conducted for several strain amplitudes. However, capturing the wide frequency range becomes problematic as TTS is not

reliable in the range of strain amplitudes where the moduli are non-constant [46]. In general this would have led to a more complex model with more time needed for material testing, with uncertain gains in accuracy.

5.1.3 Model geometry

The handball model is constructed by a perfect sphere. This sphere does not include the panels and seams present on a real handball. Earlier studies have shown that while panels and seams do affect the ball's stiffness, making it stiffer, they resulted in a maximum difference of 1.5 % from a model lacking modeled panels and seams [47]. This was thus considered an acceptable abstraction from reality to reduce modeling complexity.

5.2 Simulations and experiments

Three metrics were chosen to compare the simulation and experimental data. Peak force, impact time and outgoing velocity. The outgoing velocity is of very high importance as it indicates the momentum transfer to the HBM, which is what creates the rotational motion and accelerations causing concussions. As seen in the velocity magnitude figures of Section 4.3, the velocity magnitude after impact matches very well between simulation and experiment. There is only a slight bias towards higher exit velocities from the simulation, possibly leading to a slightly lower momentum transfer.

The impact time can also be measured from the high speed camera footage. However, due to the high velocity of the ball, 600 Frames Per Second (FPS) only captured around 6 frames during the impact. As such the impact time estimated from the footage is not very accurate, and it shows the same impact time of around 10 ms for all shots.

5.2.1 Problems with the load cell mounting

While the peak force matches quite well between shots, there is a significant amount of noise in the experimental setup. There are two major reasons for this: the entire load cell rig was mounted on a railing (cf. Figure 3.4) and the type of load cell used was not ideal.

The railing that the rig is mounted on was not rigid and could flex considerably under loading. This meant that after an impact by the ball, a lot of vibrations lingered in the structure, causing the load cell to record these vibrations as well. The peak force is still captured quite well, as the ball impact is the dominant effect during this time. After the ball departs the load cell, and the railing starts to swing back from the impact, a lot of different frequency noise is introduced. This makes it difficult to measure impact time by looking at the force data. These vibrations cause the force data to become more unreliable towards the end of the sampling

period.

The Denton 2358 load cell used in the test was not ideal for the impacts. Another load cell was planned to be used but was rendered unavailable close to when the experiment was to take place. A smaller load cell had to be used, mounted only with one machine screw in the back to a sheet metal plate. This setup did not posses the strength required to not deform by the impact from the handball. Shots hitting the 28.5 cm load cell plate off-center, caused a moment to be exerted on the mount, rotating the plate 5 - 10°. The selected shots in this study were the most centered ones, but none were perfectly centered on the plate.

5.2.2 Model confidence

The result of the load cell mounting and limited FPS of camera footage was that both the load cell data and camera footage were inadequate to measure the impact time accurately. Thus the comparison of this metric is less robust than the others, however, it does coincide well. Peak force and COR were measured with more accuracy and provide confidence in the handball model. Many impact scenarios coincide well, but there are also outliers where the percentage difference between experiment and simulation reach 10 - 20 %.

The experimental peak force is very smooth while the simulation force data contains several spikes around the peak force region. This mostly applies to the head-on impacts, cf. Figures 4.9, 4.11, 4.13 and 4.15. When these spikes coincide as peak force, they are entered into Table 4.5. They were filtered out. To create a smoother force curve, improvements in the contact modeling could be made, and the setup of the simulated aluminum wall's boundary conditions could be brought closer to reality by also modeling the fence the rig was mounted on.

The COR is consistently 5 - 10 % higher in simulations than in experiments, except for an outlier in the "Resin, angled 2" impact. This outlier might be explained by erroneous tracking data. The consistently higher COR is simply a result of the ball possessing too low damping characteristics. This could be explained by the missing viscoelasticity in the Inner layer. A possible fix could be applying a damping constant to the entire handball model or scaling up the viscous effects of the other layers to compensate. The best fix would be to conduct another material test for the Inner layer, where liquid nitrogen might not even be needed if using the Anton Paar GCU 20, which can reach $-90\,^{\circ}\mathrm{C}$ using compressed air.

5.3 HBM and handball in interaction

Concussion risk was evaluated by analyzing AIS 2 injury level across various handball impact scenarios involving a HBM. The severity of different impacts was assessed, and the surface friction between the head and the handball was examined. A simplified protective headgear was also implemented and evaluated to determine its effect

on risk of concussion.

5.3.1 Influence of impact location

The VHHI model, representing a handball impact to the HBM head at 110 km/h, yielded AIS 2 injury risk of approximately 12.5 % for impact scenario one with a friction coefficient of 0.7. Impact scenario two showed a higher risk of AIS 2 for all coefficients of friction from 0.1 to 1 in Figure 4.23. This is expected as the human head is more sensitive to rotational motion about the Z-axis than the X-axis [37]. For impact scenario two, with a friction of 0.7, the risk of AIS 2 increased to approximately 18 % which is considerably higher than for scenario one.

When compared to impact scenarios three and four in Table 4.6, even greater risks are observed. Impact scenario four represents the highest level of risk, with an AIS 2 risk value that is nearly twice as high as that of scenario two and more than two and a half times greater than the AIS 2 risk value of scenario one. These results highlight the critical importance of impact location and whether the handball's velocity vector aligns with the Z-axis of the head's center of gravity, as in impact scenario one and two. Therefore, a broader range of impact scenarios should be investigated in greater detail.

5.3.2 Influence of friction between head and handball

Figure 4.23 illustrates the influence of friction on the risk of concussion. It is evident that, for both impact scenarios one and two, the risk of AIS 2 approach zero as the coefficient of friction approaches zero. Conversely, as the coefficient of friction approaches one, the risk of AIS 2 tends towards a distinct values specific to each impact scenario.

A major increase in injury risk is observed within the friction range of 0.1 to 0.5. For coefficients of friction greater than 0.5 the risk either stabilizes or decreases slightly, though the changes are minimal. This trend underscores the critical importance of accurately determining the coefficient of friction between the handball and the head. If a sufficiently low coefficient of friction can be achieved, a substantial reduction in head injury risk may be possible.

5.3.3 Influence of damping material

Figure 4.24 shows that the stiffness of the damping material used in the protective gear within the VHSL had a relatively limited influence on the risk of concussion. However, the observed trend indicates that a decrease in material stiffness corresponds to a reduction in the risk of AIS 2 for both impact scenarios one and two. This trend is reasonable, as softer materials can absorb more impact energy and may also deform more easily, allowing them to conform better to the complex shape of the head. This could improve force distribution and reduce localized pressures that contribute to injury. Given that the risk curves continue to decline at the lowest tested stiffness level of 2 MPa, it would be of considerable interest to investigate

even softer foam materials to determine whether further reductions in head injury risk can be achieved.

5.3.4 Possible headgear evaluation

Figure 4.25 indicates that variations in friction between the sliding layers in the simplified protective gear in the VHSL model has a significant impact on the risk of concussion. When the coefficient of friction between the sliding layers is low, below approximately 0.35, the protective gear reduces the risk of concussion. In contrast, higher friction between the layers resulted in increased injury risk.

If the friction between the sliding layers is assumed to be 0.17 [41], the reduction of injury risk becomes substantial. Assuming this value for the VHSL model, the risk of AIS 2 for impact scenario one would be 9.3 %, according to Figure 4.25. For impact scenario two, the risk values are the same. This corresponds to a reduction of approximately 25 % for AIS 2 in impact scenario one. For impact scenario two, the reduction is approximately 48 %. These reductions are based on comparisons with the injury risks at a coefficient of friction of 0.8 from Figure 4.23. These results demonstrates the strong potential of protective headgear with sliding layer functionality to significantly reduce the risk of concussion.

5.3.5 Possible Sources of Error

Assumptions made in the study regarding injury prediction have led to possible sources of error, each varying in the extent to which it may influence the results. One such, concerns how the VIVA+ model is constrained. The upper body of a handball goalkeeper is not cut off and constrained as the developed FE model. However, if this affects the predicted injury risk is yet to be determined.

A further limitation with the VHSL model is the simplification of the protective gear. For instance, the model allows sliding layers to move indefinitely relative to one another. In practice, this is not the case, as most real-world protective headgear with sliding layer mechanisms imposes a limited range of motion.
Another possible source of error is the influence of pretensioned neck muscles. In a real-world scenario, a handball goalkeeper might actively tense their neck muscles in anticipation of an impact. In the FE simulations conducted in this thesis, neck muscles were not pre-tensioned. It is therefore reasonable to assume that the risk of injury could be lower in reality, as muscle activation would contribute to increased head stability and reduced head acceleration. However, this is a topic that warrants further investigation.

5.3.6 Future Development

Future development based on this study could focus on implementing a proper model of a possible protective gear in the FE model. This includes accurately determining the coefficients of friction for the implemented protective gear. Coupling this with an investigation of a wider range of impact scenarios, especially under more severe

conditions such as impact scenario four in Figure 3.8, would allow for a more comprehensive evaluation of the efficiency of protective gear.

Finally, to assess the validity of the simulation results, it is of great importance to compare them with real-world testing. Real-world throw tests performed at a crash-test dummy could be used to validate the FE model.

6
Conclusion

Material test data was collected and dynamic impact tests conducted. An FE model of a handball was developed and evaluated based on this data, and was found to be accurate to within 5 - 10 %, which was considered satisfactory. The FE model of the handball combined with the VIVA+ HBM and the DAMAGE IRF was exercised for different impact scenarios at a ball velocity 110 km/h, and concussion risks were estimated at 10 - 35 % without headgear. Injury risks compared with and without headgear showed that under the right conditions, protective headgear can substantially reduce the risk of concussion. A low friction layer between the handball and head can reduce the risk of concussion by up to 25 % for head-on impacts and 50 % for lateral impacts. With further research and development of headgear for players, it is possible to prevent lifelong injuries and make handball a safer sport.

References

[1] International Handball Federation. *New rules to be enforced in handball from 1 July 2022*. Accessed: 2025-01-30. 2022. URL: https://www.ihf.info/media-center/news/new-rules-be-enforced-handball-1-july-2022.

[2] Oxford University. *Three or more concussions linked to worse brain function in later life*. Accessed: 2025-01-21. 2023. URL: https://www.ox.ac.uk/news/2023-01-31-three-or-more-concussions-linked-worse-brain-function-later-life.

[3] Svensk Handboll. *Hjärnskakning*. Accessed: 2025-01-21. 2025. URL: https://svenskhandboll.se/handboll-i-sverige/handbollsmedicin/ledare#Hjarnskakning.

[4] Svensk Handboll. *Handbollens Spelregler 2025*. Accessed: 2025-01-21. 2025. URL: https://svenskhandboll.se/download/18.6336d09119444e6b2c36d13b/1736598071222/Handbollens_Spelregler_2025%202%20jan%202025%20g%C3%A4llande%202024-12-18%20-%20Ren%20version.pdf.

[5] V. Sturesson et al. "Youth handball concussion prevention strategies: a workshop-based study with experts and end users". In: *BMJ Open Sport & Exercise* 46 (2024). DOI: 10.1136/bmjsem-2023-001877.

[6] N. Fahse et al. "Dynamic human body models in vehicle safety: An overview". In: *GAMM-Mitteilungen* 46 (Apr. 2023). DOI: 10.1002/gamm.202300007.

[7] N. Ottosson and H. Petersson. *Introduction to the FINITE ELEMENT METHOD*. Prentice Hall Europe, 1992.

[8] Simscale. *Implicit vs Explicit Finite Element Methods (FEM)*. Accessed: 2025-02-12. 2025. URL: https://www.simscale.com/blog/implicit-vs-explicit-fem/#:~:text=Explicit%20FEM%20is%20used%20to%20calculate%20the%20state,current%20and%20later%20states%20of%20the%20given%20system.

[9] *LS-DYNA® KEYWORD USER'S MANUAL, VOLUME I and II*. URL: https://lsdyna.ansys.com/manuals/.

[10] *LS-DYNA® R14 Theory Manual*. URL: https://lsdyna.ansys.com/manuals/.

[11] M. Okereke and S. Keates. *Finite Element Applications*. First Edition. Springer Cham, 2018. ISBN: ISBN 978-3-319-67125-3. DOI: https://doi.org/10.1007/978-3-319-67125-3. URL: https://link.springer.com/book/10.1007/978-3-319-67125-3.

[12] P. Wriggers. *Computational Contact Mechanics*. Second Edition. Springer Berlin, Heidelberg, 2006. ISBN: 978-3-540-32608-3. DOI: https://doi.org/10.1007/978-3-540-32609-0. URL: https://link.springer.com/book/10.1007/978-3-540-32609-0.

[13] NASA. *Isentropic Compression (or expansion)*. Accessed: 2025-05-23. 2021. URL: https://www.grc.nasa.gov/WWW/K-12/airplane/compexp.html.

[14] *Implicit: Dynamic relaxation*. https://www.dynasupport.com/howtos/implicit/implicit-dynamic-relaxation/. Accessed: 2025-02-03.
[15] *IHF Ball Regulations*. https://www.ihf.info/sites/default/files/2021-01/Ball_Regulations_E.pdf. Accessed: 2025-02-12.
[16] J. Bergström. *Mechanics of Solid Polymers*. William Andrew Publishing, 2015.
[17] P.L. Gould. *Introduction to Linear Elasticity*. Springer New York, NY, 2015.
[18] Martin Fagerström and Magnus Ekh. *Lecture notes from TME245 Finite Element Method – Structures*. 2024.
[19] R.W. Ogden. "Large Deformation Isotropic Elasticity - On the Correlation of Theory and Experiment for Incompressible Rubberlike Solids". In: *Proceedings of the Royal Society of London. Series A, Mathematical and Physical Sciences* 326.1567 (1972), pp. 565–584. ISSN: 00804630. URL: http://www.jstor.org/stable/77930 (visited on 04/07/2025).
[20] R.M. Christensen. *Theory of Viscoelasticity (Second Edition)*. Second Edition. Academic Press, 1982. ISBN: 978-0-12-174252-2. DOI: https://doi.org/10.1016/B978-0-12-174252-2.50005-3. URL: https://www.sciencedirect.com/science/article/pii/B9780121742522500053.
[21] T-R. M. Alejandro, D-G. Mariamne, and L-U. L. Edmundo. "Prony series calculation for viscoelastic behavior modeling of structural adhesives from DMA data". In: *Ingeniería Investigación y Tecnología* (2020). DOI: 10.22201/fi.25940732e.2020.21n2.014.
[22] ZwickRoell. *Tensile Testing Machines and Testers*. Accessed: 2025-05-21. 2025. URL: https://www.zwickroell.com/products/static-materials-testing-machines/universal-testing-machines-for-static-applications/tensile-tester/.
[23] Anton Paar. *Basics of Dynamic Mechanical Analysis (DMA)*. Accessed: 2025-05-21. 2025. URL: https://wiki.anton-paar.com/en/basics-of-dynamic-mechanical-analysis-dma/.
[24] M. Mours and H.H. Winter. *Experimental Methods in Polymer Science*. Academic Press, 2000.
[25] M. Baumgaertel and H.H. Winter. "Determination of discrete relaxation and retardation time spectra from dynamic mechanical data". In: *Rheol Acta 28, 511–519* (1989). DOI: 10.1007/BF01332922.
[26] N.W. Tschoegl. *The Phenomenological Theory of Linear Viscoelastic Behavior*. Springer Berlin, Heidelberg, 1989. DOI: 10.1007/978-3-642-73602-5.
[27] K.H. Yang et al. "Development of Numerical Models for Injury Biomechanics Research: A Review of 50 Years of Publications in the Stapp Car Crash Conference". In: *Stapp Car Crash Journal, Vol. 50* (2006).
[28] R.A. Perkins et al. "Assessment of brain injury biomechanics in soccer heading using finite element analysis". In: *Brain Multiphysics* (2022).
[29] J. John et al. "Hello, world! VIVA+: A human body model lineup to evaluate sex-differences in crash protection". In: *Frontiers in Bioengineering*

and Biotechnology 10 (2022). DOI: 10.3389/fbioe.2022.918904. URL: https://www.frontiersin.org/articles/10.3389/fbioe.2022.918904.

[30] *Viva+ Publications*. https://vivaplus.readthedocs.io/en/latest/model/publications/. Accessed: 2025-01-30.

[31] VIVA+ Team. *VIVA+ Human Body Models — Model Design*. https://vivaplus.readthedocs.io/en/latest/model/. Accessed: 2025-05-22. 2025.

[32] T. Wu et al. "Integrating Human and Nonhuman Primate Data to Estimate Human Tolerances for Traumatic Brain Injury". In: *Journal of Biomechanical Engineering* 144.7 (Feb. 2022), p. 071003. ISSN: 0148-0731. DOI: 10.1115/1.4053209. eprint: https://asmedigitalcollection.asme.org/biomechanical/article-pdf/144/7/071003/6846854/bio_144_07_071003.pdf. URL: https://doi.org/10.1115/1.4053209.

[33] Association for the Advancement of Automotive Medicine. *Abbreviated Injury Scale 2015 Revision*. Barrington, IL: AAAM, 2015.

[34] Rong Huang, Justin Smith, and Yi Zhou. "A comprehensive review of head injury criterion (HIC) and its role in traumatic brain injury (TBI) evaluation". In: *Procedia Computer Science* 174 (2020), pp. 314–329. DOI: 10.1016/j.procs.2020.06.082. URL: https://www.sciencedirect.com/science/article/pii/S1877056820300678.

[35] V.G. Khurana and A.H. Kaye. "An overview of concussion in sport". In: *Journal of Clinical Neuroscience* (2011).

[36] D. King et al. "Assessment, Management and Knowledge of Sport-Related Concussion: Systematic Review". In: *Sports Medicine* 44.4 (2014), pp. 449–471.

[37] E.G. Takhounts et al. "Development of Brain Injury Criteria (BrIC)". In: *Stapp Car Crash Journal, Vol. 57* (2013).

[38] R. Willinger, C. Deck, and N. Bourdet. "Helmet standards and design: current limitations and future directions". In: *Proceedings of the Institution of Mechanical Engineers, Part P: Journal of Sports Engineering and Technology* 233.1 (2019), pp. 45–60. DOI: 10.1177/1754337118778244.

[39] Lauren M. McNamara, Thomas A. Gennarelli, and Elliot J. Pellman. "Impact performance of modern snow sport helmets: Influence of liner foam composition and design". In: *Journal of Biomechanics* 105 (2020), p. 109791. DOI: 10.1016/j.jbiomech.2020.109791.

[40] Mips AB. *What Does Mips Mean?* https://mipsprotection.com/what-does-mips-mean/. Accessed: 2025-05-23. 2025.

[41] Yong Han et al. "Quantitative analysis of the protective performance of bicycle helmet with multi-direction impact protection system in oblique impact tests". In: *Chinese Journal of Traumatology* 27.4 (2024), pp. 226–234. ISSN: 1008-1275. DOI: https://doi.org/10.1016/j.cjtee.2024.03.002. URL: https://www.sciencedirect.com/science/article/pii/S1008127524000282.

[42] M. Springer. *PYVISCO: A Python library for identifying Prony series parameters of linear viscoelastic materials*. Version 1.0.2. 2022. DOI: 10.5281/zenodo.7672127. URL: https://github.com/NREL/pyvisco.

[43] R.W. Ogden. *Non-linear Elastic Deformations*. Ellis Horwood series in mathematics and its applications. E. Horwood, 1984. ISBN: 9780853122739. URL: https://books.google.se/books?id=-pEeAQAAIAAJ.

[44] R.M. Christensen. "A Nonlinear Theory of Viscoelasticity for Application to Elastomers". In: *Journal of Applied Mechanics* 47.4 (Dec. 1980), pp. 762–768. ISSN: 0021-8936. DOI: 10.1115/1.3153787. eprint: https://asmedigitalcollection.asme.org/appliedmechanics/article-pdf/47/4/762/5878877/762_1.pdf. URL: https://doi.org/10.1115/1.3153787.

[45] Corina Klug et al. *Dynasaur: Dynamic Simulation Analysis of Numerical Results*. Version 1.0. Vehicle Safety Institute, Graz University of Technology. 2018. URL: https://gitlab.com/VSI-TUGraz/Dynasaur.

[46] A. Oseli et al. "Time-Temperature Superposition in Linear and Non-linear Domain". In: *Materials Today: Proceedings* 3.4 (2016). 32nd DANUBIA ADRIA SYMPOSIUM on Advanced in Experimental Mechanics, pp. 1118–1123. ISSN: 2214-7853. DOI: https://doi.org/10.1016/j.matpr.2016.03.059. URL: https://www.sciencedirect.com/science/article/pii/S2214785316002649.

[47] D.S. Price, R. Jones, and A.R. Harland. "Computational modelling of manually stitched soccer balls". In: *Proceedings of the Institution of Mechanical Engineers, Part L* 220.4 (2006), pp. 259–268. DOI: 10.1243/14644207JMDA83.

A

Material test specimen data

Table A.1: Test specimens used in the tensile test. Gauge length is the free length between the clamps

Material sample	Gauge length [mm]	Width [mm]	Thickness [mm]
Outer	14.8047	12.5	1.3
Foam	14.9897	11.0	3.5
Inner	20.0574	10.8	1.0
Bladder	15.3614	11.0	1.3

Table A.2: Test specimens used in the DMA

Material sample	Total length [mm]	Width [mm]	Thickness [mm]
Outer	51	11.3	1.3
Foam	46	11.7	3.5
Inner	43	12.9	1.0
Bladder	40	12.6	1.3

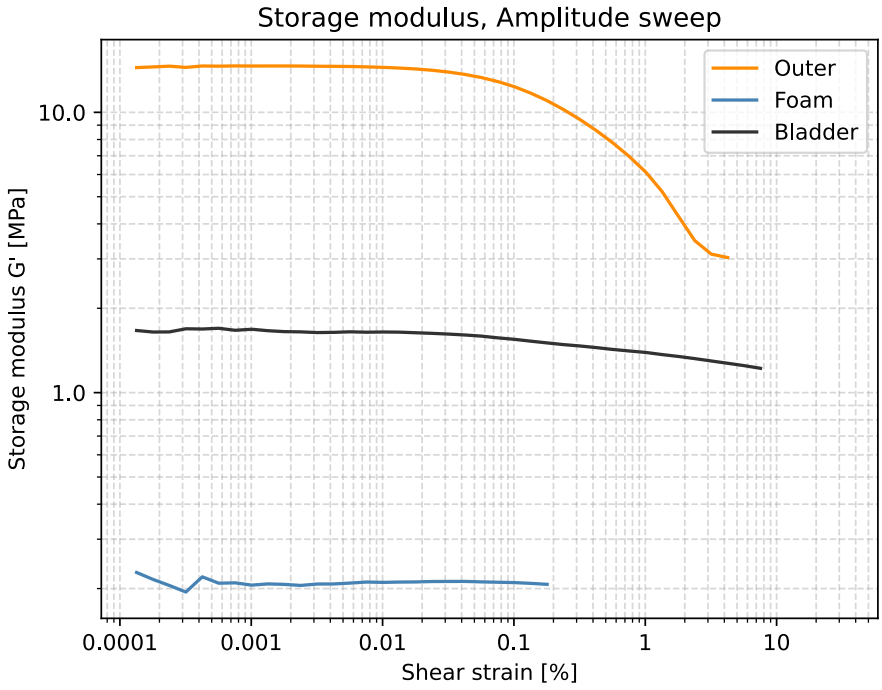

Figure A.1: Amplitude sweep showing storage modulus drop for higher strain amplitudes

DEPARTMENT OF MECHANICS AND MARITIME SCIENCES
CHALMERS UNIVERSITY OF TECHNOLOGY
Gothenburg, Sweden 2025
www.chalmers.se

CHALMERS
UNIVERSITY OF TECHNOLOGY